Nature Communications

https://doi.org/10.1038/s41467-025-67674-9

Article in Press

Intraperitoneal programming of tailored CAR macrophages via mRNA lipid nanoparticle to boost cancer immunotherapy

Received: 24 February 2025

Accepted: 4 December 2025

Cite this article as: Gu, K., Liang, T., Hu, L. *et al.* Intraperitoneal programming of tailored CAR macrophages via mRNA lipid nanoparticle to boost cancer immunotherapy. *Nat Commun* (2025). https://doi.org/10.1038/s41467-025-67674-9

Kedan Gu, Ting Liang, Luting Hu, Yifan Zhao, Weiyang Ying, Mengke Zhang, Yashuang Chen, Benmeng Liang, Xinrui Lin, Yanqi Zhang, Hongyu Wu, Meng Wang, Yuping Zhu, Wenxi Wang, Yu Zhang, Chao Zuo, Zhen Du, Penghui Zhang, Jia Song, Liwen Li, Xiangsheng Liu, Sitao Xie & Weihong Tan

Title: Intraperitoneal programming of tailored CAR macrophages *via* mRNA lipid nanoparticle to boost cancer immunotherapy

Authors: Kedan Gu,[1,2] Ting Liang,[1] Luting Hu,[1] Yifan Zhao,[1] Weiyang Ying,[1] Mengke Zhang,[1] Yashuang Chen,[1] Benmeng Liang,[3] Xinrui Lin,[3] Yanqi Zhang,[3] Hongyu Wu,[1] Meng Wang,[1] Yuping Zhu,[1] Wenxi Wang,[1,2] Yu Zhang,[1,2,4] Chao Zuo,[1,2,4] Zhen Du,[1,2] Penghui Zhang,[1,2] Jia Song,[3] Liwen Li,[1] Xiangsheng Liu,[1,2*] Sitao Xie,[1,2,4,5*] Weihong Tan[1,2*]

Affiliations:

[1]Zhejiang Cancer Hospital, The Key Laboratory of Zhejiang Province for Aptamers and Theranostics, Hangzhou Institute of Medicine (HIM), Chinese Academy of Sciences; Hangzhou, 310022, China.

[2]School of Molecular Medicine, Hangzhou Institute for Advanced Study, University of Chinese Academy of Sciences; Hangzhou, 310024, China.

[3]Institute of Molecular Medicine (IMM), Renji Hospital, Shanghai Jiao Tong University School of Medicine, College of Chemistry and Chemical Engineering, Shanghai Jiao Tong University; Shanghai, 200240, China.

[4]Zhejiang Key Lab of Vaccine, Infectious Disease Prevention and Control, Zhejiang Provincial Center for Disease Control and Prevention, Hangzhou, 310015, China

[5]Molecular Science and Biomedicine Laboratory (MBL), State Key Laboratory of Chemo/Biosensing and Chemometrics, College of Chemistry and Chemical Engineering,

College of Biology, Aptamer Engineering Center of Hunan Province, Hunan University; Changsha, 410082, China.

*Corresponding author. Email: tan@him.cas.cn; xiesitao@him.cas.cn; liuxs@him.cas.cn

Abstract: Therapeutic strategies for peritoneal metastasis in solid tumors are urgently needed. Programming chimeric antigen receptor macrophages (CAR-Ms) *in situ* offers opportunities for an unmet demand. However, potential intracellular domains (ICDs) for CAR design and their antitumor mechanisms for macrophage empowerment remain to be explored systematically. By developing a macrophage-targeted mRNA lipid nanoparticle (mRNA-LNP) system, we evaluate 36 CAR formats in CAR-Ms. Tailored CAR-Ms with CD3ζ TLR4 ICDs elicit robust adaptive immune activation and significantly synergize with PD-1/L1 therapy. Single-cell RNA sequencing (scRNA-seq) reveals that CAR-Ms reshape the immunosuppressive tumor microenvironment (TME) and boost the $TCF1^{+}PD\text{-}1^{+}$ progenitor-exhausted $CD8^{+}$ T cells (Tpex) population. Mechanistically, CAR-Ms maintain a proinflammatory phenotype and simultaneously upregulate MHC-I and PD-L1 by perturbing NF-κB pathways. Collectively, this approach enables intraperitoneal programming of tailored CAR-Ms and broadens understanding of both regulatory and feedback mechanisms for CAR-M therapies against solid tumors.

INTRODUCTION

Peritoneal metastasis in solid tumors poses significant clinical challenges in oncology[1]. A typical combination of cytoreductive surgery (CRS) and hyperthermic intraperitoneal chemotherapy (HIPEC) provides benefits to a minority of patients with

minimal tumor burdens[1,2]. At the same time, it is not considered a clinical option for the majority of patients with advanced peritoneal tumors[3,4]. Immunotherapy represents a promising frontier for addressing peritoneal metastasis[5]. However, peritoneal tumors often develop evasive mechanisms against the immune system, resulting in disease progression and unfavorable outcomes[6,7]. Hence, there is a clinically urgent and unmet need to explore alternative immunotherapies for the majority of peritoneal metastasis patients.

Meanwhile, peritoneal ascites from peritoneal metastasis patients harbor a substantial population of immune cells, with macrophages constituting approximately 45%[8]. As for the tumor microenvironment (TME), tumor-associated macrophages (TAMs) are roughly categorized into proinflammatory M1-like or pro-tumoral M2-like up to 50% of total cells[9,10]. High levels of M2-like TAM infiltration are often associated with poor prognosis and resistance to immunotherapy in clinical trials[11,12]. Therefore, approaches to altering the phenotype or function of macrophages to enhance immune responses against solid tumors are under investigation[13-20].

In particular, CAR macrophages (CAR-Ms) exhibit a pronounced phagocytic activity toward target cells and can easily penetrate solid tumors, demonstrating decreased tumor burden and prolonged overall survival in preclinical solid tumor models[21-27]. However, the elaborate and costly manufacturing processes similar to those FDA-approved CAR-T[21,25,28], when coupled with the tumorigenic risk[29,30] of viral vector-involved cell engineering, restrict the accessibility of CAR-Ms to patients who would otherwise benefit from the broader clinical applications. In response, researchers began trying to generate CAR-Ms *in vivo* to treat solid tumors directly by constructing non-viral nanocarriers[31].

Concurrently, considering the various barriers and complexities of metabolic distribution associated with intravenous infusion[32,33], we speculate that it should be a more feasible way to administer mRNA-LNP for CAR-M therapy intraperitoneally.

Furthermore, current research on the architecture of the intracellular domain (ICD) of macrophages primarily focuses on CD3ζ signal transduction. Yet, exclusive reliance on CD3ζ is far from fully exploiting the multifunctional characteristics of macrophages for tumor immunotherapies. Orchestrated through an array of natural receptors, macrophages sense and respond to external cues, executing multifaceted roles that encompass phagocytosis, immunomodulation and antigen presentation. Noteworthy among these receptors, the recognition of β-glucans by the C-type lectin receptor Dectin1 underscores the pivotal role of macrophages in fungal defense mechanisms[34,35]. By engaging with its ligand CD40L, the CD40 receptor facilitates transition towards the proinflammatory M1 phenotype[36,37], thereby asserting immune homeostasis. Additionally, recognition of lipopolysaccharides (LPS) by Toll-like receptors TLR2 and TLR4 triggers intracellular signaling cascades[38] that culminate in activating proinflammatory pathways. CD46 is a well-known viral magnet, and CSF2R is common to IL-3, IL-5 and GM-CSF receptors. However, whether these natural receptor ICDs could be designed to functionalize CAR-M in a manner similar to CD3ζ remains to be elucidated. Thus, systematically investigating the rational design, combination, and biological effects of signaling pathways implicated in macrophages through the CAR modality is in order.

In this work, we explore the biological effects of 36 CAR combinations (Supplementary Table 1) containing diverse ICDs (Phagocytosis: CD3ζ and Dectin1; proinflammatory: CD40 and TLR4; and possible effector: CD46 and CSF2R) on

macrophages *in vitro* and *in vivo*. By developing a targeted mRNA-LNP delivery system for macrophages, we achieve highly efficient *in vivo* construction of CAR-Ms required for cancer immunotherapy. In two syngeneic solid tumor mouse models, intraperitoneal programming of tailored CAR-Ms elicits robust adaptive immune system activation and significantly synergizes with standard-of-care PD-1/PD-L1 immune checkpoint blockade (ICB) therapy in resistant models. Further analysis by comprehensive single-cell RNA sequencing (scRNA-seq) demonstrates that in vivo programming of CAR-Ms with CD3ζ TLR4 ICDs significantly promotes the transition of macrophages from an M2 to an M1 proinflammatory phenotype and is accompanied by perturbations of the NF-κB pathway that upregulate PD-L1 and major histocompatibility complex class I (MHC I). In addition, we find that CAR-Ms reshape the immunosuppressive tumor microenvironment, thereby boosting the population of $TCF1^{+}PD\text{-}1^{+}$ progenitor exhausted CD8 T cells (Tpex). Furthermore, the synergistic effect between siRNA-mediated knockdown of PD-L1 and CAR-Ms highlights the critical role of PD-L1 expression on macrophages in antigen cross-presentation process.

RESULTS

Functional design and optimization of CARs for CAR-M

Phosphatidylserine, as the macrophage-specific uptake unit[39], and β-sitosterol to improve mRNA transfection[40] were incorporated in the existing mRNA-based lipid nanoparticles (LNP) delivery system to form phosphatidylserine/β-sitosterol LNP (termed “PSβ-LNP”) (Fig. 1a), which could perform mRNA transfection to various macrophage cell types with high efficiency (Supplementary Fig. 1a-1b). The expression of a series of CAR

constructs in primary macrophages was validated by flow cytometry (Fig. 1b). Confocal imaging indicated that the mRNA-encoded CARs could be localized on the cell membrane (Fig. 1c). PSβ-LNP was characterized as having an average diameter of 164 ± 0.7 nm, a polydispersity index (PDI) of less than 0.1, and a pKa of around 6.72, demonstrating a controllable particle size distribution and endosomal escape capabilities at the cellular level (Supplementary Fig. 1c-1f).

To ascertain the functionality potentially mediated by the designed CARs, CAR-Ms were generated from transfected BMDMs using corresponding CAR mRNA encapsulated within the PSβ-LNP. Subsequently, macrophages and luciferase-expressing tumor cells were cocultured and analyzed as depicted in Fig. 1d. It should be noted that Dectin1 CAR-M eradicated tumor cells in an E:T (effector cells: target cells) ratio-dependent manner similar to that of CD3ζ CAR-M (Fig. 1e), further noting that its phagocytic activity was not dependent on the amount of CAR-encoding mRNA (Supplementary Fig. 2a). In comparison, CD3ζ CAR-M exhibited significantly higher activity at the 10:1 ratio (Fig. 1e). Additional imaging analysis showed that the pHrodo™ Red-labeled tumor cells emitted bright red fluorescence in the CD3ζ or Dectin1 CAR-M group, suggesting that engulfed tumor debris was degraded in acidic phagolysosome lumen (Supplementary Fig. 2b). Flow cytometry data indicated a more vital interaction between CD3ζ or Dectin1 CAR-Ms and tumor cells by the proportion of calculated changes of 20.5% or 17.4%, respectively, compared to the untreated (UTD) group of 7.0% (Fig. 1f). Antigen-specific beads engulfment assay further demonstrated successful CAR-M phagocytosis (Fig. 1g and Supplementary Fig. 2c-2e). Furthermore, we observed a marked elevation of proinflammatory cytokines, including IL-6, IL-12 and TNF-α, in the supernatant of the

CD40 or TLR4 CAR-M treated group (Fig. 1h, 1i and Supplementary Fig. 2f). Next, CAR-Ms were further analyzed to explore the relationship between CAR effects and gene changes. RNA-seq principal component analysis (PCA) and featured interferon-associated genes heatmap revealed that CD3ζ showed a gene signature similar to that of Dectin1, whereas CD40 was similar to TLR4 (Fig. 1j, 1k and Supplementary Fig. 3). Heightened expression of the IL-12 gene was only detected in the CD40 and TLR4 groups in alignment with the findings from cytokine analysis in the supernatant (Fig. 1h and 1k). The stimulation induced by empty LNP, deemed negligible, was similar to that of the UTD group in the coculture system. Neither the CD46 nor CSF2R CAR design appeared to mediate much discernible functionality since no significant difference was observed compared to that of either UTD or Empty groups, especially in featured genes (Fig. 1j and 1k). Gene ontology (GO) analysis suggested that four functional CARs for CAR-M mediated activation of innate immune response (Supplementary Fig. 3). Taken together, CD3ζ or Dectin1 CARs primarily mediated macrophage with enhanced phagocytosis functionalities, while CD40 or TLR4 CARs induced more marked proinflammatory regulation.

To improve the antitumor performance of CAR-M, we further optimized the ICD and extracellular domain (ECD) of CARs. Considering the temporal limitation of mRNA-encoding CAR and the potential degradation of CAR structure after target antigen recognition, we introduced a lysine-to-arginine (K-R) mutation in the ICD (Fig. 2a and Supplementary Table 2), a strategy inspired by CAR-T to stabilize CAR expression *via* impairing CAR ubiquitination[41]. $CAR^{K\text{-}R}$ and CAR^{K} exhibited similar metabolic profiles in the presence of target tumor cells. Despite the consistently higher positivity rate of $CAR^{K\text{-}}$

^{R} at each time point of detection, the difference compared to the CAR^{K} was statistically marginal (Fig. 2b and 2c). As for ECD optimization, given the revealed coordinative transcriptional regulation and expression of CD47 and HER2[42,43], together with the pivotal role of the CD47–SIRPα axis in suppressing macrophage phagocytosis, we engineered a mutated SIRPα[44] as a high-affinity CD47 antigen recognition domain of the CAR construct to block the native CD47-SIRPα interaction and thereby enhance phagocytosis (Fig. 2a). With an E:T ratio of 10:1, the αCD47 CAR markedly augmented CAR-M phagocytosis to near-eradication of all tumor cells, whereas about 25% of tumor cells remained alive in the αHER2 CAR-M group (Fig. 2d and Supplementary Fig. 4a). With CD47- and HER2-positive or -negative tumor cells as target, it is confirmed that phagocytic activation could potentially be triggered by stimulation through either CD47 or HER2 (Fig. 2e-2g and Supplementary Fig. 4b). IncuCyte-based assays demonstrated the continuous and specific phagocytic process up to 72 hours (Fig. 2h, 2i and Supplementary movies).

Intraperitoneal programming of CAR-M *via* mRNA PSβ-LNP

Initially, we validated the nucleic acid delivery capability of GFP-mRNA PSβ-LNP towards macrophages in a colon cancer CT26 syngeneic mouse model with peritoneal metastasis according to the protocol outlined in Fig. 3a. In malignant ascites, macrophages accounted for approximately 45% of the total peritoneal cells in the PSβ-LNP group, and more than 60% of these macrophages were GFP-positive, indicating efficient transfection within 18 hours after a single administration, significantly surpassing the efficiency observed with traditional LNPs (Fig. 3b and 3c). Additionally, we observed that the total cell count in the peritoneal fluid was higher in LNP group compared to the

control group (40–65 million vs. 20 million, Supplementary Fig. 5a), along with a corresponding rise in the proportion of macrophages (Fig. 3b). For tumor itself, three-quarters of all transfected cells were F4/80-positive and approximately 23% of intratumoral F4/80-positive cells were transfected (Supplementary Fig. 5b). Regarding the spatial distribution of transfected cells, further immunofluorescent (IF) sections revealed that widespread eGFP expression primarily appeared in macrophages within the tumor, ranging from the periphery to the interior (Fig. 3d). In ascites, macrophages accounted for more than 80% of the mRNA-transfected cell population, while a small fraction of monocytes and dendritic cells were also transfected, and lymphocytes were rarely transfected (Fig. 3e), suggesting preferential selectivity and transfection efficiency of PSβ-LNP towards macrophages. This high degree of macrophage targeting was consistently observed in both the colorectal and pancreatic cancer models. To further evaluate the PSβ-LNP biodistribution, we also examined the organ distribution of PSβ-LNP after intraperitoneal administration. DIR-labeled PSβ-LNP predominantly accumulated at the tumor lumps and livers following intraperitoneal injection, with minimal dispersion outside the peritoneal cavity and other organs (Fig. 3f and Supplementary Fig. 5c-5d). This pattern was consistently observed in both colorectal and pancreatic cancer models, including both peritoneal dissemination and orthotopic settings. Similar results were also observed in the ovarian cancer SKOV3 xenograft mouse model (Supplementary Fig. 5e-5f). Furthermore, we investigated the *in vivo* persistence of CAR expression. In the absence of target antigens, CAR maintained a relatively high positivity rate. However, under continuous stimulation with an excess of surface antigens, the proportion of CAR-positive cells dropped to less than 5% at 40 hours (Fig. 3g).

Encouraged by the above *in situ* transfection assay results, we further monitored the antitumor capacity of CAR-mRNA encapsulated within PSβ-LNP in the CT26-luc syngeneic mouse model (Fig. 3h). Results revealed potent tumor inhibitory effects for both CD3ζ CAR-M and Dectin1 CAR-M, significantly prolonging the survival of tumor-bearing mice (Fig. 3i). It should be noted that CD3ζ CAR demonstrated superior therapeutic efficacy compared to Dectin1 CAR, while no observable therapeutic effects were achieved in the Empty LNP group. During the early stages of treatment, the CAR-M group experienced a brief period of weight loss, followed by sustained growth (Supplementary Fig. 6a), indicating a minor and tolerable toxicity from mRNA-LNP. In the later stages of observation, control mice exhibited significant abdominal distension and rough fur. At the same time, the CAR-M treatment group did not display these symptoms (Supplementary Fig. 6b). Prior major depletion of macrophages was achieved in mice using clodronate liposomes (Supplementary Fig. 6c) before intervention abolished the therapeutic benefits of subsequent CAR-mRNA PSβ-LNP administration (Fig. 3j-3l), underscoring the essential role of macrophages in the programming of CAR-M using CAR-mRNA PSβ-LNP *in vivo*. In summary, we comprehensively validated the *in vivo* macrophage-targeting capability, efficient mRNA delivery of PSβ-LNP, and the preliminary antitumor efficacy of CAR-mRNA LNP.

CAR-Ms activate the adaptive immune system and sensitize αPD-1 therapy

Considering this pivotal role of macrophages in the intricate innate and adaptive immune response network, we conducted further investigations to evaluate the influence of *in situ* generation of CAR-M on the immune system. To investigate the potential of CAR-M intervention in establishing sustained adaptive immune protection, we re-

challenged mice, which had previously achieved complete tumor eradication following CAR-M treatment, by administering one million tumor cells subcutaneously (Fig. 4a). Over a prolonged observation period, these tumors were once again wholly inhibited (Fig. 4a and 4b), confirming comprehensive adaptive immune protection in mice. Additionally, to elucidate the impact of CAR-M intervention on antigen-specific T cells, we harvested splenocytes from mice and stimulated them with tumor cells for an enzyme-linked immunospot assay (ELISPOT) assay. Based on ELISPOT assay, the number of tumor-specific T cells in cured mice was significantly elevated compared to naive mice (1,118 vs. 253 tumor-specific T cells detected per 1.5×10^5 splenocytes) (Fig. 4c), indicating that CAR-M intervention enhances the proliferation of antigen-specific T cells. Moreover, the adoptive transfer of 10 million splenocytes from these cured mice to naive mice resulted in a pronounced inhibition of tumor growth (Fig. 4d). These experimental results provide compelling evidence for the activation of adaptive immunity by *in situ* CAR-M. However, once the tumor microenvironment (TME) was fully established, the adoptive transfer of splenocytes from cured mice demonstrated only a marginal tumor suppression (Fig. 4e), which could be partly attributed to the limited ability of tumor-specific T cells to infiltrate the tumor interior (Fig. 4f).

Considering the proinflammatory characteristics of CD40 CAR and TLR4 CAR in macrophages, we further combined them with the phagocytic-promoting CD3ζ and evaluated their properties in an immunocompetent mouse model with a more advanced tumor (Fig. 4h-4i). Transfecting macrophages with two mRNAs simultaneously resulted in a high percentage of dual-positive cells, demonstrating efficient co-transfection. (Supplementary Fig. 7a). We found that the parallel constructs (CD3ζ CD40 or CD3ζ

TLR4) exhibited more significant tumor-suppressive effects (Fig. 4h and Supplementary Fig. 7b). Notably, the peritoneal fluid from mice treated with TLR4 CAR or the parallel sequences showed a marked increase in type 1 helper T cells and $CD8^+$ reactive T cells (Fig. 4j), indicating that the parallel CARs effectively activated the adaptive immune system. Furthermore, the highest M1 to M2 macrophage ratio was observed in ascites and tumors treated with the parallel CAR (Fig. 4j and Supplementary Fig. 7c-7d), suggesting that the parallel can promote maintenance of the M1 phenotype. A comprehensive assessment of extracellular cytokine release levels demonstrated higher levels of proinflammatory cytokine release in all parallels containing TLR4 CAR (Supplementary Fig. 8). Moreover, we noted that the parallel CD3ζ TLR4 CAR demonstrated superior tumor phagocytic capacity *in vitro* compared to the parallel CD3ζ CD40 CAR (Supplementary Fig. 9a and 9b). However, the underlying mechanism appears to differ from the previously observed TLR agonist-induced activation of the pBTK/CRT pathway, which resulted in calreticulin translocation to the cell membrane and enhanced the phagocytic effect of CD47 antibodies (Supplementary Fig. 9c-9e).

In light of potent activation of the adaptive immune system by tailored CARs in tandem, such as parallel CD3ζ TLR4 CAR and parallel CD3ζ CD40 noted above, we further explored tailored CAR-M with PD-1/PD-L1 immune checkpoint therapy. It is noteworthy that the CT26 mouse syngeneic tumor model is typically regarded as insensitive to PD-1 antibodies. However, in our hands PD-1 antibody and CAR-M treatment separately demonstrated mild antitumor growth effects in late-stage CT26 intraperitoneal tumors (Fig. 5a and 5b). Surprisingly, the combination of PD-1 antibody and CAR-M (termed as “Comb”) led to almost complete eradication during a brief dosing

period and significantly improved mouse survival rates (Fig. 5a-5c). To procure sufficient tumor tissue for subsequent analysis, dosing initiation was delayed until day 12 post-tumor inoculation. The intervention demonstrated a trend consistent with that observed previously (Supplementary Fig. 10a). In addition, we also demonstrated that this strategy is equally effective in orthotopic tumor models (Supplementary Fig. 10b-10c). Within the CAR-M treatment group, the proportion of M1 phenotype in tumor lumps was highest (Fig. 5d). In contrast, the combination treatment group showed significantly increased T-cell infiltration, especially $CD8^+$ T cells (Fig. 5e and Supplementary Fig. 10d). To comprehensively illustrate the changes in cellular composition within the TME, multicolor immunofluorescence staining was performed (Fig. 5f). In the untreated group, immune cell numbers were significantly lower, both at the core and periphery of the tumor mass, compared to other experimental groups. In the αPD-1 group, a substantial increase in myeloid cell infiltration was observed. However, the CAR-M and Comb groups exhibited diverse immune cell presence in marginal and internal tumor tissues. The wide-ranging changes in cell types are closely associated with the secretion of multiple cytokines. Meanwhile, higher levels of IL-12 were detected in the blood in the CAR-M and Comb treatment groups (Fig. 5g), indicating a milieu conducive to multiple immune cells, particularly cytotoxic T cells. To demonstrate such variable cytokine secretion, we further conducted a Luminex assay for cytokine cluster analysis (Fig. 5h). In hierarchical clustering, we observed consistent trends in intertumoral cytokine release between the CAR-M and Comb with upregulation of clustered cytokines (CCL1, CCL11, CXCL10, CXCL11, and IFN-γ) compared to control, or αPD-1. Multiple studies have highlighted that IFN-γ-induced chemokines, such as CXCL10 and CXCL11, play a crucial role in

eliciting chemotaxis[45-47], especially of monocytes/macrophages and T cells within the TME. In summary, CAR-M intervention led to reshaping the cellular and cytokine landscape of the TME, fostering substantial immune activation to support T cell functionality.

Since CD47 is a pan-cancer target, we applied the same treatment in the PAN02 pancreatic cancer model. Interestingly, transient monotherapy with CAR-Ms alone demonstrated robust tumor eradication capabilities, while the PD-1 antibody was utterly ineffective (Fig. 5i and 5j). Nonetheless, we observed that the synergistic effect of CAR-Ms combined with PD-1 antibodies still resulted in delayed tumor recurrence and a marked extension of overall survival (Fig. 5i, 5j and Supplementary Fig. 10e). Therefore, it appeared that CAR-Ms could sensitize PD-1/PD-L1 blockade therapy, making ICB a broadly applicable therapeutic option.

Furthermore, we compared the performance of the CD3ζ TLR4 CAR with the CD3ζ CAR in the presence of a PD-1 inhibitor (Supplementary Fig. 11). The results showed that the parallel CAR exhibited stronger M1 polarization capability and a greater ability to mobilize T cells, as evidenced by reduced T cell numbers in the spleen and increased T cell accumulation in the lymph nodes.

Regarding safety, mouse weight changes were also within the normal range (Supplementary Fig. 10f-10g). We did not detect intervention-related liver or kidney dysfunction (Supplementary Fig. 12) or organic lesions in treated mice (Supplementary Fig. 13). While we observed a reduction in red blood cell and platelet counts associated with targeting CD47, the overall red blood cell count remained within the safety baseline

(Supplementary Fig. 14 and Supplementary Table 3). In short, CAR-Ms could activate adaptive immunity, especially parallel CD3ζ TLR4 CARs, showing particularly strong effects. In addition, the tailored CAR-Ms combined with PD-1 antibodies demonstrated powerful synergistic effects and manageable toxicity in various PD-1/L1-resistance models.

Synergism mechanism between CAR-M and ICB

To further elucidate the interaction between CAR-M and PD-1/L1 ICB therapy, single-cell RNA sequencing (scRNA-seq) was performed to analyze the changes of immune cells within the TME during the treatment of CT26 mouse syngeneic tumor model (Fig. 6a). After data filtering and quality control, we analyzed 8,467, 13,845, 13,986, and 14,933 immune cells in the UTD, αPD-1, CAR-M and Comb, respectively. Cell annotation showed shifts in immune cell proportions after various treatments with increased T cells and granulocytes in the CAR-M and combination therapy groups compared to αPD-1 monotherapy or UTD, along with a decrease in macrophage populations compared to αPD-1 treatment (Fig. 6b). Notably, macrophage cluster 1, which comprised most CAR-M and Comb, demonstrated the highest M1 scores and the lowest M2 scores (Fig. 6c-6d and Supplementary Fig. 15) characterized by the downregulation of *Trem2* and the upregulation of *Cd80* and *Nos2* (Fig. 6e), and meanwhile the cluster 1 was in the minority in the αPD-1 treatment. These data align with prior findings (Fig. 4j and 5d), indicating that CAR-M effectively maintained the antitumor phenotype *in vivo*.

Indeed, studies suggested that up to 75% of tumor PD-L1 could be derived from macrophages[48,49]. We noted that macrophage cluster 1 demonstrated a significant

upregulation of the PD-L1 gene (*Cd274*) compared to other clusters (Fig. 6e), a finding consistent with our *in vitro* observations of increased PD-L1 expression in macrophages following CAR signaling (Fig. 6f). Additionally, we observed a substantial upregulation of MHC I molecules and MHC-associated gene expression in macrophages (Fig. 6f-6h), which may contribute to the improved infiltration of $CD8^+$ T cells *via* antigen cross-presentation within the TME. In an *in vitro* coculture system containing functional CAR-Ms and tumor cells, we found that PD-L1 expression in tumor cells was also significantly upregulated. At the same time, MHC I expression in both colorectal and pancreatic cancer cells showed only slight changes (Supplementary Fig. 16). In comparison, the upregulation of PD-L1 in tumor cells was substantially higher than that in macrophages, suggesting that tumor cells exhibit a significantly stronger negative immunoregulatory response to external interventions (Supplementary Fig. 17). Considering prior studies indicating a correlation between NF-κB pathway activation and PD-L1 and MHC I expression[50], we reviewed previous GO (Gene Ontology) analysis data, which indicated the activation of the NF-κB pathway following CAR transduction (Supplementary Fig. 18a). Additionally, we confirmed that the CAR signaling-induced increase in PD-L1 and MHC I could be abolished by NF-κB pathway inhibitors or IKKβ-siRNA (Fig. 6i and Supplementary Fig. 18b-18d). While the upregulation of MHC I could enhance the efficacy of immunotherapy, its full therapeutic potential may be contingent upon concurrent PD-L1 blockade (Fig. 6j). Although disrupting the PD-L1/PD-1 axis in dendritic cells and T cells is critical, our results indicated that siRNA-mediated knockdown of substantial PD-L1 in macrophages could synergize effectively with simultaneous CAR-M therapy (Fig. 6k and Supplementary Fig. 19).

In addition to conducting a systematic and comprehensive analysis of macrophages, we examined T cells in the TME. All T cell populations within the tumor exhibited significant upregulation of exhaustion markers *Tox* and *Pdcd1* (Fig. 6l and Supplementary Fig. 20). The PD-1 antibody monotherapy group contained a higher proportion of effector T cells. In contrast, the CAR-M and Comb were enriched with terminally exhausted T cells, proliferative T cells and progenitor-exhausted T cells (Tpex) (Fig. 6l and Supplementary Fig. 20). Of particular significance was the observation that CAR-M proved advantageous in promoting the formation of Tpex clusters. Recent studies have indicated that Tpex populations are the predominant responders to PD-1 ICB[51-53], highlighting their relevance in immunotherapy.

In summary, we elucidated the mechanisms underlying the potent synergism between tailored CAR-M and PD-1 antibodies (Fig. 6m). CAR-M, stimulated by tumor antigens, retained an M1 phenotype and upregulated MHC I and PD-L1 through the NF-κB pathway. Following the degradation of tumor cell debris by CAR-M, extensive antigen cross-presentation was performed, significantly enriching the Tpex population responsive to PD-1/PD-L1 antibodies. Moreover, the administration of PD-1 antibodies mitigated the adverse effects of PD-L1 upregulation, thereby fully liberating Tpex cells. Ultimately, CAR-M and Tpex constituted an effective cellular population against tumor cells.

DISCUSSION

The diverse range of responses exhibited by solid tumor patients undergoing T cell-related immunotherapy highlights the necessity for exploring alternative treatment strategies. Macrophages, as critical regulators within the TME, profoundly influence

therapeutic outcomes in solid tumors. Strategies for modulating the phenotype or function of macrophages to potentiate the immune microenvironment against solid tumors are currently under investigation. In peritoneal metastasis, the peritoneal cavity harbors a substantial reservoir of macrophages. Our approach, involving the intraperitoneal infusion of CAR-mRNA PSβ-LNP, facilitated the rapid and extensive generation of tumor-targeting multifunctional CAR-Ms with variable ICDs within the cavity. Consequently, upon tumor recognition, these engineered macrophages demonstrated tumor phagocytosis *via* CD3ζ- or Dectin1-mediated intracellular signaling, concurrently triggering the release of proinflammatory cytokines through TLR4 or CD40 signaling. This dual mechanism maintained an M1-like proinflammatory phenotype in macrophages, further activating and mobilizing the adaptive immune system. In two mouse syngeneic models resistant to PD-1/PD-L1 ICB, tailored CAR-Ms exhibited significant synergistic effects with PD-1 antibodies, attributed partly to TME reshaping and Tpex population expansion induced by CAR-Ms. Moreover, it was essential to emphasize that CAR signaling led to the activation of the NF-κB pathway, subsequently increasing the expression of both MHC I and PD-L1. The upregulation of MHC I on cancer cells could sensitize cancer cells to T cell-dependent killing[50]. Meanwhile, pMHC on the macrophage for presentation to T cells could serve as the primary event required for T cell activation[54]. Previous studies have emphasized the inhibitory effect of PD-L1 on dendritic cells (DCs) on T cell immunity[48,49], while our results indicated that the PD-L1 on *in situ* prepared CAR-Ms is also crucial for adequate T cell activation, underscoring the necessity of combining CAR-Ms with PD-1 ICB therapy. Furthermore, we demonstrated that the parallel CD3ζ TLR4 CAR-Ms in combination with a PD-1 antibody maintained a higher M1 macrophage population and

achieved greater T cell mobilization compared with the recently reported combination of the CD3ζ CAR-Ms and a PD-1 antibody[55].

To optimize phagocytosis, incorporating CD47 blockade into the CAR ECD significantly enhanced phagocytosis, with controllable hematotoxicity observed. This highlights the need to explore preferential recognition of tumor cell CD47 over that on red blood cells[56,57]. Following excessive antigen stimulation, CAR expression was downregulated in macrophages. This downregulation may be attributable to activation-induced internalization and degradation of CAR molecules. In fact, the expression dynamics of CARs in macrophages remain to be further investigated, particularly the changes that occur upon target antigen stimulation. To achieve durable CAR-M persistence, K-R mutations were introduced into the CAR ICD to resist ubiquitination. However, the results indicate that these mutations provide limited improvement in CAR-M persistence. Therefore, further structural optimization of the CAR design will be necessary to achieve long-term CAR expression following a single CAR-mRNA LNP administration, which is a critical prerequisite for the clinical translation of mRNA-LNPs given their 'hit-and-run' mode of action. In addition, the distribution of PSβ-LNPs in the liver may represent a double-edged sword, as it could help prevent liver metastasis while simultaneously raising concerns about hepatotoxicity, although liver and kidney functions remained normal after short-term administration.

In conclusion, we developed an mRNA-LNP delivery system for efficient intraperitoneal programming of tailored CAR-Ms for advanced peritoneal-disseminated late-stage tumors. *In situ* programming of CAR-Ms, especially for parallel CD3ζ TLR4 CAR-Ms, exhibits promising therapeutic potential, demonstrating powerful synergistic

effects with traditional ICB therapy and significant promise for clinical translation. Moving forward, we aim to undertake a comprehensive evaluation of the antitumor efficacy and pharmacokinetic profile of *in situ* programming CAR-M within organoid models and non-human primate (NHP) systems.

METHODS

Ethics statement. All mouse studies complied with the humane and ethical treatment of experimental animals and were approved by the Hangzhou Institute of Medicine, Chinese Academy of Science Animal Center. All mice used in this study were obtained from the Zhejiang Experimental Animal Center. All mice were housed in a clean, pathogen-free, and humid environment at 25 °C with a typical humidity level of 50%, under a 12-hour dark/12-hour light cycle, with sufficient sterile water and food supply. Mice were euthanized when tumors reached 20 mm in any direction or 2000 mm^3 volume, whichever occurred first. No mice exceeded these limits before euthanasia.

Cells and culture conditions. Cell lines THP-1, HS578T, MDA-MB-231, RAW264.7, 4T1 and CT26 used in this study were purchased from ATCC. SKOV3-luc, CT26-luc and ID8-luc were purchased from iCell. KPC-luc was a kind gift from the Penghui Zhang laboratory from HIM. eGFP and luciferase-containing GV260 lentiviral vectors (Ubi-eGFP-Firefly Luciferase-Ires Puromycin, Genechem) were transfected into HS578T and MDA-MB-231 for stable HS578T-luc and MDA-MB-231-luc cell lines as previously described. Briefly, cells were seeded at appropriate density, incubated with the lentiviral particles for 24 h, and subsequently selected with puromycin (1 μg/mL). Human ERBB2 (HER2), eGFP, and luciferase-containing lentiviral vectors (Ubi-HER2-eGFP-Firefly Luciferase-IRES-

Puromycin, Genechem) were transfected into CT26 and 4T1 for stable CT26-eGFP-luc-HER2 and 4T1-eGFP-luc-HER2 cell lines. All cell lines were cultured in complete RPMI-1640 with 10% origin FBS (Gibco), 1% penicillin/streptomycin (Gibco) and grown at 37 °C and 5% CO_2 with saturating humidity. Bone marrow-derived macrophages (BMDMs) were generated as previously described with minor modification[58]. In brief, single-cell supernatants collected from murine femurs were cultured in complete RPMI-1640 with 20 ng/mL M-CSF (Sangon) for 7 days to harvest M0 macrophages and 20 ng/mL IL-4 (Sangon) for another 2 days to harvest M2a macrophages. All cell lines were routinely tested for mycoplasma contamination every two weeks. In addition, prior to tumor cell implantation *in vivo*, mycoplasma testing was performed according to the animal facility's requirements to ensure that no contamination occurred.

mRNA construction and synthesis. The CARs in this study are composed of antigen-binding domain (scFv from Trastuzumab or mutated SIRPα), CD8α hinge, transmembrane domain, and intracellular domains from CD3ζ, CD40, CD46, CSF2R, Dectin1, and TLR4. Responding codon-optimized CAR plasmid was constructed with a T7 promoter, 5'-UTR and 3'-UTR, CAR sequence and poly (A)-tail. After linearization *via* restriction endonuclease BspQI, purified DNA was used as a template to transcribe CAR-mRNA *via* a T7 High Yield RNA Transcription Kit (Novoprotein). Notably, to avoid immune responses to foreign nucleic acids caused by intracellular immune sensors in macrophages, all designed mRNAs were modified with N1-methyl-pseudouridine to lower immunogenicity[59]. IVT mRNA capped with a Cap 1 Capping System Kit (Novoprotein) was purified and diluted to 1 μg/μL for standby.

Construction and characterization of mRNA-LNP. mRNAs diluted in citrate buffer (pH 4.0) were encapsulated in lipid nanoparticles (LNP) *via* self-assembly. Briefly, lipids, including ethanol containing ionizable cationic lipid (SM102), phosphatidylcholine (DSPC), cholesterol analogs (β-sitosterol), polyethylene glycol-lipid (DMG-PEG2000) and phosphatidylserine (DOPS) (molar ratio: 50:10:34:1:5), and mRNA in citrate buffer (pH 4.0) were mixed rapidly as volume ratio 1:2 and flow rate 20 mL/min *via* the microfluidic platform INano™ E (Micro&Nano). After pH balance and ultrafiltration, mixed mRNA-LNPs were stored at 4 °C for subsequent characterization and evaluation within 3 days. The physicochemical properties of RNA-loaded particles, including radius and polydispersity, were characterized by Zetasizer (Malvern). The morphology of particles was characterized by transmission electron microscope (TEM, JEM-2100plus from JEOL). Efficacy of the encapsulated particles was assessed *via* a Quant-iT™ RiboGreen™ RNA Assay Kit (Thermo Fisher). Theoretical calculation of pKa of particles was characterized *via* a TNS binding assay. Virtual lysosomal escape capability (membrane fusion and destabilization) was characterized *via* hemolysis assay at neutral and acidic pH, as described previously[60]. Briefly, human RBCs were incubated with LNPs at 37 °C for 1 h in either PBS or citrate buffer (pH 5.5), after which hemolysis was assessed by centrifugation and measurement of supernatant absorbance at 540 nm.

Transfection of macrophages. After being seeded in wells for 8–12 hours, macrophages (BMDMs or RAW264.7) were co-cultured with mRNA-LNPs (typically 1 μg mRNA per 1.0×10^6 cells) in complete medium at 37 °C. For suspension cells such as THP-1, transfection was performed immediately after cell preparation. Transfection efficiency was analyzed using eGFP or CAR expression proportionally by flow cytometry

(Beckman Coulter, CytoFLEX) and microscopy (Olympus ckx53). CARs were labeled with HER2 protein-conjugated Alexa Fluor 647 or MonoRab™ GS Linker Antibody (PE) (A02314-100, GenScript). The gating strategy for flow cytometry analysis is provided in Supplementary Fig. 21.

Beads-based phagocytosis assay. HER2-PS beads were obtained from carboxylated polystyrene spheres (Bangs Laboratories) coupled with HER2 protein *via* crosslinkers 1-ethyl-3-(3-dimethylaminopropyl) carbodiimide hydrochloride (EDC) and N-hydroxy succinimide (NHS). 18 h after transfection, CAR-Ms were cocultured with PS-HER2 beads (ratio: 1:10) for 1 h at 37 °C. The uptake was stopped immediately by lowering the temperature. Beads-based phagocytosis was characterized *via* microscopy (TECAN). For quantitative analysis *via* flow cytometry (Beckman Coulter), HER2-PS beads were conjugated with fluorescein isothiocyanate (FITC), and macrophages were stained with the lipophilic membrane labeling probe 1,1'-dioctadecyl-3,3,3',3'-tetramethylindocarbocyanine perchlorate (DIL) dye (Beyotime).

***In vitro* cytotoxicity assay.** After being plated in white flat non-transparent wells (Corning), BMDMs were transfected with the corresponding CAR-mRNA (1 μg mRNA into 1.0 million BMDMs). Following 18 hours of transfection, luciferase-loaded tumor cells were added in various E:T ratios, systematically adjusted from 10:1 to 1:1. After incubating for a total of 24 hours, bioluminescence luciferase substrate (D-Luciferin sodium salt, APExBIO) was added to achieve a final concentration of 1.5 mg/mL, and the luminescence signal was measured within 10 minutes using a microplate reader (TECAN Spark). For imaging with IVIS Spectrum, the white wells were replaced with black transparent wells (Corning). To image the engulfment of debris by macrophages, tumor

cells were labeled with pHrodo™ Red (Invitrogen™). For the phagocytosis process study, CAR-M and GFP-loaded tumor cells were monitored *via* Incucyte SX5 (Satorius), and images were captured every one and a half hours for three days.

Cytokine analysis. After being plated in white flat non-transparent wells (Corning), BMDMs were transfected with the corresponding CAR-mRNA (1 μg mRNA into 1.0 million BMDMs). Following 18 hours of transfection, tumor cells were added proportionally at an E:T ratio of 5:1. After incubating for a total of 12 hours, the supernatant was collected from medium and subsequently diluted with 1× DPBS at different multiples. Secretion of cytokines (IL-6, IL-12, TNF-α) was tested using the corresponding ELISA assay kit (Sangon Biotech) and analyzed by a microplate reader (TECAN Spark).

RNA sequencing of macrophages. After coculturing BMDM/CAR-Ms and targeted tumor cells or blank control for 12 hours, total RNA was extracted and isolated. The raw image data from sequencing results were processed using the Bcl2fastq software (v2.17.1.14) for base calling. Cutadapt (version 1.9.1) was used to preprocess the raw data, filtering out low-quality data and removing contamination and adapter sequences. Short reads were aligned using the Hisat2 (v2.0.1) software with default parameters. RNA-Seq data were analyzed for differential alternative splicing using rMATS (version 4.1.0). Based on the alignment results of each sample to the reference genome, the samtools (v0.1.19) software was used for mpileup processing to obtain potential SNV results for each sample. Subsequently, the annovar (v2016.05.11) software was used for annotation. Gene expression was calculated using HTSeq software (v0.6.1), which utilizes the FPKM (Fragments Per Kilobase per Million reads) method to quantify gene

expression levels. We filtered the detected results according to the criteria of significant differential expression (fold change in gene expression of 2 or more and q-value ≤ 0.05).

Mice and *in vivo* tumor models.

To model peritoneal metastasis CRC tumors, 2.0×10^5 colorectal cancer tumor cells CT26-luc were intraperitoneally injected (i.p.) into Balb/c mice (4 to 6 weeks old). An ovarian tumor CDX model was built *via* inoculation (i.p.) of 3.0×10^6 SKOV3 cells into immunodeficient nude mice. To model peritoneal metastasis in pancreatic tumors, 1.0×10^6 PAN02-luc cells were intraperitoneally injected (i.p.) into C57BL/6 mice (4 to 6 weeks old).

To determine target and transfection efficacy, GFP-mRNA/CAR-mRNA LNP or DIR-labeled LNP was injected (i.p.) 9~11 days after inoculation in both CT26 and PAN02 syngeneic mouse models. The dosage used for testing was 10 μg of mRNA or an equivalent dose of LNP with sampling for analysis after 16 hours. Uptake signal, transfection signal and distribution profile of various cell types, including macrophage (F4/80+), T cell (CD3+), monocyte (CD11c-Ly6G-F4/80-), DC (CD11c+F4/80-Ly6G-), NK cell (NK1.1+ for CT26 model or NKp46+ for PAN02 model), B cell (CD19+) were characterized by GFP and DIR, respectively, *via* flow cytometry, IF, and IVIS. Primary antibodies used in the flowcytometry study are listed as follows: F4/80 (111604, BioLegend), CD3 (100218, BioLegend), Ly6G (E-AB-F1108UQ, Elabscience), CD11c (117318, BioLegend), NKp46 (3201878, Invitrogen), NK1.1 (E-AB-F0987Q, Elabscience), CD19 (557399, BD).

To evaluate CAR expression persistence in the presence or absence of antigen stimulation, CAR-mRNA (anti-HER2 CAR or anti-CD47 CAR) LNP was injected intraperitoneally in CT26 syngeneic mouse models. The dosage used for testing was 10 μg of mRNA. Expression of the CAR element containing a GS linker in peritoneal macrophages was analyzed at 16, 24, 32, and 40 hours after a single CAR-mRNA LNP injection.

For the antitumor efficacy study, CAR-mRNA PSβ-LNP was injected (i.p.) daily (5 μg/mouse) from the 3rd day after the inoculation of tumor cells, and tumor growth was monitored every three days by bioluminescence imaging (IVIS Lumina Series III, PerkinElmer) and analyzed using Living Image v4.4 (Caliper Life Sciences).

To evaluate the role of macrophages in mediating the therapeutic efficacy of mRNA-LNPs, macrophage depletion was performed using clodronate liposomes (SunLipo NanoTech, SN-ML-E005) according to the manufacturer's instructions. Briefly, 200 μL of 5 mg/mL clodronate liposomes was diluted to a final volume of 400 μL per mouse and administered via intraperitoneal injection. 24 hours or 72 hours after injection, peritoneal ascites was collected, and depletion efficiency (F4/80 positive percent) was assessed by flow cytometry.

For the rechallenge study, 1.0×10^6 tumor cells were injected (s.c.), and tumor growth was monitored every other day. The weight of mice was recorded every three days. At the experiment endpoint, mice were euthanized in accordance with laboratory animal guidelines.

For the tumor challenge experiment using splenic cell adoptive transfer from cured mice, 10 million splenic cells from cured mice were intravenously injected into naive mice one day before tumor implantation, followed by subcutaneous implantation of 1 million tumor cells. Tumor growth in mice was recorded every other day.

For the immune challenge experiment in an established TME, 1 million tumor cells were implanted (s.c.) in advance. On the seventh day after implantation, 10 million splenic cells from cured mice were adoptively transferred. Tumor growth in mice was then monitored every other day.

To evaluate the effect of single CAR or parallel CAR in situ programming of CAR-M therapy in the CT26-luc syngeneic model, treatment was initiated on day 9 after intraperitoneal implantation of 2.0×10^5 CT26-luc tumor cells. The dosing regimen was as follows: CAR-mRNA PSβ-LNP was administered intraperitoneally once daily for a total of seven doses. The daily mRNA dose per mouse was 5.0 μg for the CD3ζ CAR group, 2.5 μg for the CD40 CAR or TLR4 CAR groups, and 7.5 μg for the parallel CAR groups (comprising 5 μg of CD3ζ CAR mRNA and 2.5 μg of either CD40 or TLR4 CAR mRNA).

To evaluate the combined antitumor effects of PD-1 antibody and *in situ* programming of CAR-M therapy in the CT26-luc syngeneic model, intervention started on the 9th day after implantation of 2.0×10^5 CT26-luc tumor cells (i.p.). The dosing regimen was as follows: PD-1 antibody was administered (i.p.) every three days at a dose of 100 μg per mouse per administration, totaling three administrations. CAR-mRNA PSβ-LNP was administered (i.p.) once daily with a total daily mRNA dose of 7.5 μg per mouse (comprising 5 μg of CD3ζ CAR mRNA and 2.5 μg of TLR4 CAR mRNA), totaling seven

administrations. The combination group received both CAR-mRNA treatment and PD-1 antibody treatment with a total daily mRNA dose of 7.5 μg per mouse and PD-1 antibody at a dose of 100 μg (i.p.) every three days per mouse. Tumor growth was monitored every three days using IVIS. In the orthotopic tumor model, 1.0×10^5 CT26 cells were inoculated, and intervention with combination treatment began on day 7 post-inoculation. Intervention in the later-stage tumor model began on the 12th day to ensure an adequate supply of tumor samples for subsequent IF analysis, Luminex assay and scRNA sequencing.

To evaluate the combined effects in the PAN02-luc syngeneic model, the intervention started on the 8th day after implantation of 1.0×10^6 PAN02-luc tumor cells (i.p.). Intervention and monitoring measures were identical to those described above. Briefly, PD-1 antibody was administered (i.p.) every three days at 100 μg per mouse for three doses, while CAR-mRNA PSβ-LNP was administered (i.p.) once daily for seven consecutive days with a total daily mRNA dose of 7.5 μg per mouse (5 μg CD3ζ CAR mRNA and 2.5 μg TLR4 CAR mRNA). The combination group received both regimens as described.

To evaluate the combined antitumor effects of siRNA-mediated macrophage PD-L1 knockdown and *in situ* programming of CAR M therapy, PD-L1 siRNA was administered (i.p.) starting on the 8th day after tumor implantation at a dose of 5 μg per mouse every three days, totaling three administrations, and CAR-mRNA PSβ-LNP was administered starting on the 9th day with a total mRNA dose of 7.5 μg per mouse per day (comprising 5 μg of CD3ζ CAR mRNA and 2.5 μg of TLR4 CAR mRNA), totaling seven administrations. The combination group received both of CAR-mRNA treatment and PD-

L1 siRNA treatment as described. Tumor growth was monitored every three days using IVIS. The sequences of PD-L1 siRNAs are listed in Supplementary Table 4.

TME and peripheral immune system study. Peritoneal ascites was collected for the tumor microenvironment study, and tumors were resected for immunohistochemical analysis and then tumors, spleens and lymph nodes were digested for flow cytometry after red blood cell lysis. Immune cell panels were stained with anti-mouse flow cytometry antibody probes. Macrophage polarization was checked *via* M1 (F4/80+CD80+) or M2 (F4/80+CD206+) markers after intervention. T cell phenotypes, including T_{naive} (CD62L+CD44-), $T_{effector}$ (CD62L-CD44+), Th1 (CD4+IFNγ+), CD8 reactive T cell (CD8+IFNγ+), $T_{activated}$ (CD3+CD25+). Primary antibodies used in the study are listed as follows: F4/80 (123117, BioLegend), F4/80 (111604, BioLegend), CD80 (50446-R014-A-25, Sino Biological), CD206 (FAB2535P, R&D), CD206 (#24595, CST), CD3 (100228, BD), CD3e (561108, BD), CD4 (550954, BD), CD8 (K0227-A64, MBL), CD25 (564021, BD), CD44 (103025, BioLegend), CD62L (104405, BioLegend), IFNr (505807, BioLegend), and goat anti-rabbit IgG H&L (Alexa Fluor® 488) (ab150077, abcam). All collected data were analyzed using FlowJo 10.8.1 software.

In addition, the secretion of multiple cytokines was tested *via* a Luminex assay. The hierarchical clustering plot was generated using the R software (v.4.2.2) package ape (v.5.6.2)[61] through Hiplot Pro (https://hiplot.com.cn/), a comprehensive web service for biomedical data analysis and visualization.

T cell activation and IFNγ ELISPOT. T cells collected from ascites and tumors were stained with flow cytometry antibody probes. Activated $CD8^+$ T cells were determined as

$CD3^+CD8^+IFNr^+$, and TH1 cells were determined as $CD3^+CD4^+IFN\gamma^+$. For the rechallenge study, an ELISPOT assay was performed to evaluate T-cell activation. In summary, 1.5×10^5 splenocytes collected from cured mice or naïve mice after RBC lysis were seeded in wells of a 96-well IFNγ ELISPOT plate with 1.5×10^4 tumor cells to stimulate tumor-specific T cells. After incubation for 18 hours, the ELISpot assay was conducted utilizing the IFN-γ ELISpot kit (ThermoFisher) in accordance with the manufacturer's instructions. Spots were captured under an automated ELISpot and FluoroSpot reader (Mabtech Astor2).

Tumor and spleen digestion. The excised tumors and spleens were cut into small pieces of approximately 3 mm^3. Then, these small pieces were incubated in a Collagenase/Hyaluronidase (10X collagenase/hyaluronidase in DMEM, STEMCELL) solution for one hour before passing through a 300-mesh cell strainer. The targeted single-cell population was obtained after RBC lysis and centrifugation.

PD-L1 and MHC-I upregulation after CAR signal transduction. 18 hours after CAR-mRNA transfection, tumor cells were cocultured with CAR-Ms or control macrophages for an additional 12 hours. The collected cells were then stained with anti-F4/80 (123117, BioLegend), anti-CD274 (558091, BD; 1:100 dilution), and either anti-H-2Kb/H-2Db (114605, BioLegend; 1:100 dilution) or anti-H-2Kd (2841476, Invitrogen; 1:100 dilution) for flow cytometry analysis.

To assess PD-L1 and MHC-I expression following CAR signal transduction under NF-κB pathway perturbation, IKKβ-siRNA LNP (1 μg per 1×10^6 macrophages) was transfected into macrophages 24 hours prior to CAR-mRNA transfection. The sequence

of KKβ-siRNA is listed in Supplementary Table 4. For pathway inhibition using a NF-kBi, NF-kBi (Pyrrolidinedithiocarbamate ammonium, PDTC, 100 μM) was added to the medium during coculture of CAR-Ms and tumor cells.

Single-cell RNA-seq. Single-cell counting and quality control were performed using the TC20 Automated Cell Counter (Bio-Rad, USA). Then, after GEM (Gel Bead-in-emulsion) generation, 10x barcoded, full-length cDNA amplification was obtained from polyadenylated mRNA. After library construction, all repositories with different indices were multiplexed and loaded on an Illumina NovaSeq instrument according to the manufacturer's instructions (Illumina, San Diego, CA, USA). Raw sequencing data quality control and mapping were performed with a 10X genomics single-cell gene expression analysis pipeline. Subsequently, cell quality control, clustering, and marker gene analysis were performed using Seurat (v4.3.0). We excluded genes expressed in only a small number of cells to maintain the quality of genes and cells. Then, SingleR (v2.0.0) was utilized for cell type annotation. GOSeq (v1.34.1) was employed for Gene Ontology (GO) enrichment analysis, in-house scripts were used for KEGG (Kyoto Encyclopedia of Genes and Genomes) enrichment analysis, reactomPA (v1.42.0) was used for reactome pathway enrichment, and GSVA (v1.46.0) was applied for gene set variation analysis (GSVA). Additionally, Monocle was utilized to infer the pseudotime trajectory of cells.

All software used for single-cell RNA analysis in the study was listed as Supplementary Table 5.

Biocompatibility. To evaluate biosafety, 7.5 μg CAR-mRNA PSβ-LNP or an equivalent dose of empty LNP was injected intraperitoneally into healthy Balb/c mice daily. After 7

consecutive days, the mice were euthanized. Primary organs, including heart, liver, lung, kidney, spleen, and intestine, were collected for H&E staining and pathological analysis, and corresponding blood was collected for blood biochemistry and routine blood tests. Blood counts were performed *via* an automatic hematology analyzer (BC-2800vet, Mindary).

Statistics. All data analyses were conducted using GraphPad Prism (v 8.0) with results presented as mean ± SD. P-values were determined using one/two-way analysis of variance (ANOVA) for tumor growth, followed by multiple comparison tests as indicated in the figure captions. Spearman's rho correlation test was used to assess correlations, a log-rank test was used for survival analysis, and unpaired two-tailed t-tests were used for other analyses. A P-value less than 0.05 was considered statistically significant. Experiments were repeated multiple times as independent trials.

Data availability. Source data are provided with this paper. The main data supporting the results in this study are available within the paper and its Supplementary Information. The single-cell RNA sequencing data can be accessed from the Genome Sequence Archive (GSA) under the accession number CRA023627 (https://ngdc.cncb.ac.cn/gsub/submit/gsa/subCRA038363/finishedOverview), and the bulk RNA sequencing data under accession number CRA023617 (https://ngdc.cncb.ac.cn/gsub/submit/gsa/subCRA038350/finishedOverview). Additional raw dataset, mRNA template and cell lines described in this study are available upon request from the corresponding author (Prof. Sitao Xie, xiesitao@him.cas.cn) and subject to an executed Materials Transfer Agreement with Hangzhou Institute of Medicine (HIM), Chinese Academy of Sciences.

References

1 Kepenekian, V. *et al.* Advances in the management of peritoneal malignancies. *Nat Rev Clin Oncol* **19**: 698-718. (2022).
2 Cortes-Guiral, D. *et al.* Primary and metastatic peritoneal surface malignancies. *Nat Rev Dis Primers* **7**: 91. (2021).
3 Coccolini, F. *et al.* Peritoneal carcinomatosis. *World J Gastroenterol* **19**: 6979-6994. (2013).
4 Cao, C. *et al.* A systematic review and meta-analysis of cytoreductive surgery with perioperative intraperitoneal chemotherapy for peritoneal carcinomatosis of colorectal origin. *Ann Surg Oncol* **16**: 2152-2165. (2009).
5 Morano, W. F. *et al.* Intraperitoneal immunotherapy: historical perspectives and modern therapy. *Cancer Gene Ther* **23**: 373-381. (2016).
6 Yao, X. *et al.* Molecular biology and immunology of gastric cancer peritoneal metastasis. *Transl Gastroenterol Hepatol* **5**: 57. (2020).
7 Ornella, M. S. C. *et al.* Immunotherapy for Peritoneal Carcinomatosis: Challenges and Prospective Outcomes. *Cancers (Basel)* **15**. (2023).
8 Kubicka, U. *et al.* Normal human immune peritoneal cells: subpopulations and functional characteristics. *Scand J Immunol* **44**: 157-163. (1996).
9 Duan, Z. *et al.* Targeting macrophages in cancer immunotherapy. *Signal Transduct Target Ther* **6**: 127. (2021).
10 Biswas, S. K. *et al.* Macrophage plasticity and interaction with lymphocyte subsets: cancer as a paradigm. *Nat Immunol* **11**: 889-896. (2010).
11 Pittet, M. J. *et al.* Clinical relevance of tumour-associated macrophages. *Nat Rev Clin Oncol* **19**: 402-421. (2022).
12 Zhang, H. *et al.* Roles of tumor-associated macrophages in anti-PD-1/PD-L1 immunotherapy for solid cancers. *Mol Cancer* **22**: 58. (2023).
13 Hao, Y. *et al.* The CD47-SIRPalpha axis is a promising target for cancer immunotherapies. *Int Immunopharmacol* **120**: 110255. (2023).
14 Anderson, N. R. *et al.* Macrophage-Based Approaches for Cancer Immunotherapy. *Cancer Res* **81**: 1201-1208. (2021).
15 Barkal, A. A. *et al.* CD24 signalling through macrophage Siglec-10 is a target for cancer immunotherapy. *Nature* **572**: 392-396. (2019).
16 Majeti, R. *et al.* CD47 is an adverse prognostic factor and therapeutic antibody target on human acute myeloid leukemia stem cells. *Cell* **138**: 286-299. (2009).
17 Feng, Y. *et al.* A toll-like receptor agonist mimicking microbial signal to generate tumor-suppressive macrophages. *Nat Commun* **10**: 2272. (2019).
18 Zhang, F. *et al.* Genetic programming of macrophages to perform anti-tumor functions using targeted mRNA nanocarriers. *Nat Commun* **10**: 3974. (2019).
19 Jalil, A. R. *et al.* Macrophage checkpoint blockade: results from initial clinical trials, binding analyses, and CD47-SIRPalpha structure-function. *Antib Ther* **3**: 80-94. (2020).
20 Joshi, S. *et al.* Tim4 enables large peritoneal macrophages to cross-present tumor antigens at early stages of tumorigenesis. *Cell Rep* **43**: 114096. (2024).
21 Klichinsky, M. *et al.* Human chimeric antigen receptor macrophages for cancer immunotherapy. *Nat Biotechnol* **38**: 947-953. (2020).
22 Kang, M. *et al.* Nanocomplex-Mediated In Vivo Programming to Chimeric Antigen Receptor-M1 Macrophages for Cancer Therapy. *Adv Mater* **33**: e2103258. (2021).
23 Gao, L. *et al.* Convection-enhanced delivery of nanoencapsulated gene locoregionally yielding ErbB2/Her2-specific CAR-macrophages for brainstem glioma immunotherapy. *J Nanobiotechnology* **21**: 56. (2023).
24 Chen, C. *et al.* Intracavity generation of glioma stem cell-specific CAR macrophages primes locoregional immunity for postoperative glioblastoma therapy. *Sci Transl Med* **14**: eabn1128. (2022).
25 Lei, A. *et al.* A second-generation M1-polarized CAR macrophage with antitumor efficacy. *Nat Immunol*. (2023).

26 Shen, J. *et al.* Activating innate immune responses repolarizes hPSC-derived CAR macrophages to improve anti-tumor activity. *Cell Stem Cell* **31**: 1003-1019 e1009. (2024).
27 Li, N. *et al.* A new era of cancer immunotherapy: combining revolutionary technologies for enhanced CAR-M therapy. *Mol Cancer* **23**: 117. (2024).
28 Blache, U. *et al.* Potential solutions for manufacture of CAR T cells in cancer immunotherapy. *Nat Commun* **13**: 5225. (2022).
29 Spanjaart, A. M. *et al.* Confused about Confusion. *N Engl J Med* **386**: 80-87. (2022).
30 Lareau, C. A. *et al.* Latent human herpesvirus 6 is reactivated in CAR T cells. *Nature* **623**: 608-615. (2023).
31 Yang, Z. *et al.* Dual mRNA co-delivery for in situ generation of phagocytosis-enhanced CAR macrophages augments hepatocellular carcinoma immunotherapy. *J Control Release* **360**: 718-733. (2023).
32 Poon, W. *et al.* A framework for designing delivery systems. *Nat Nanotechnol* **15**: 819-829. (2020).
33 Sindhwani, S. *et al.* The entry of nanoparticles into solid tumours. *Nat Mater* **19**: 566-575. (2020).
34 Taylor, P. R. *et al.* Dectin-1 is required for beta-glucan recognition and control of fungal infection. *Nat Immunol* **8**: 31-38. (2007).
35 Theobald, H. *et al.* Apolipoprotein E controls Dectin-1-dependent development of monocyte-derived alveolar macrophages upon pulmonary beta-glucan-induced inflammatory adaptation. *Nat Immunol*. (2024).
36 Vonderheide, R. H. CD40 Agonist Antibodies in Cancer Immunotherapy. *Annu Rev Med* **71**: 47-58. (2020).
37 Liu, P. S. *et al.* CD40 signal rewires fatty acid and glutamine metabolism for stimulating macrophage anti-tumorigenic functions. *Nat Immunol* **24**: 452-462. (2023).
38 Kagan, J. C. *et al.* TRAM couples endocytosis of Toll-like receptor 4 to the induction of interferon-beta. *Nat Immunol* **9**: 361-368. (2008).
39 Luozhong, S. *et al.* Phosphatidylserine Lipid Nanoparticles Promote Systemic RNA Delivery to Secondary Lymphoid Organs. *Nano Lett* **22**: 8304-8311. (2022).
40 Patel, S. *et al.* Naturally-occurring cholesterol analogues in lipid nanoparticles induce polymorphic shape and enhance intracellular delivery of mRNA. *Nat Commun* **11**: 983. (2020).
41 Li, W. *et al.* Chimeric Antigen Receptor Designed to Prevent Ubiquitination and Downregulation Showed Durable Antitumor Efficacy. *Immunity* **53**: 456-470 e456. (2020).
42 Candas-Green, D. *et al.* Dual blockade of CD47 and HER2 eliminates radioresistant breast cancer cells. *Nat Commun* **11**: 4591. (2020).
43 Upton, R. *et al.* Combining CD47 blockade with trastuzumab eliminates HER2-positive breast cancer cells and overcomes trastuzumab tolerance. *Proc Natl Acad Sci U S A* **118**. (2021).
44 Weiskopf, K. *et al.* Engineered SIRPalpha variants as immunotherapeutic adjuvants to anticancer antibodies. *Science* **341**: 88-91. (2013).
45 Hoch, T. *et al.* Multiplexed imaging mass cytometry of the chemokine milieus in melanoma characterizes features of the response to immunotherapy. *Sci Immunol* **7**: eabk1692. (2022).
46 Reschke, R. *et al.* CXCL9 and CXCL10 bring the heat to tumors. *Sci Immunol* **7**: eabq6509. (2022).
47 Chow, M. T. *et al.* Intratumoral Activity of the CXCR3 Chemokine System Is Required for the Efficacy of Anti-PD-1 Therapy. *Immunity* **50**: 1498-1512 e1495. (2019).
48 Oh, S. A. *et al.* PD-L1 expression by dendritic cells is a key regulator of T-cell immunity in cancer. *Nat Cancer* **1**: 681-691. (2020).
49 Peng, Q. *et al.* PD-L1 on dendritic cells attenuates T cell activation and regulates response to immune checkpoint blockade. *Nat Commun* **11**: 4835. (2020).
50 Gu, S. S. *et al.* Therapeutically Increasing MHC-I Expression Potentiates Immune Checkpoint Blockade. *Cancer Discov* **11**: 1524-1541. (2021).
51 Im, S. J. *et al.* Defining CD8+ T cells that provide the proliferative burst after PD-1 therapy. *Nature* **537**: 417-421. (2016).
52 Tsui, C. *et al.* MYB orchestrates T cell exhaustion and response to checkpoint inhibition. *Nature* **609**: 354-360. (2022).
53 Siddiqui, I. *et al.* Intratumoral Tcf1(+)PD-1(+)CD8(+) T Cells with Stem-like Properties Promote Tumor Control in Response to Vaccination and Checkpoint Blockade Immunotherapy. *Immunity* **50**: 195-211 e110. (2019).

54 Guerriero, J. L. Macrophages: Their Untold Story in T Cell Activation and Function. *Int Rev Cell Mol Biol* **342**: 73-93. (2019).
55 Pierini, S. *et al.* Chimeric antigen receptor macrophages (CAR-M) sensitize HER2+ solid tumors to PD1 blockade in pre-clinical models. *Nat Commun* **16**: 706. (2025).
56 Qu, T. *et al.* Ligufalimab, a novel anti-CD47 antibody with no hemagglutination demonstrates both monotherapy and combo antitumor activity. *J Immunother Cancer* **10**. (2022).
57 Yu, J. *et al.* SIRPalpha-Fc fusion protein IMM01 exhibits dual anti-tumor activities by targeting CD47/SIRPalpha signal pathway via blocking the "don't eat me" signal and activating the "eat me" signal. *J Hematol Oncol* **15**: 167. (2022).
58 Trouplin, V. *et al.* Bone marrow-derived macrophage production. *J Vis Exp*: e50966. (2013).
59 Andries, O. *et al.* N(1)-methylpseudouridine-incorporated mRNA outperforms pseudouridine-incorporated mRNA by providing enhanced protein expression and reduced immunogenicity in mammalian cell lines and mice. *J Control Release* **217**: 337-344. (2015).
60 Miao, L. *et al.* Synergistic lipid compositions for albumin receptor mediated delivery of mRNA to the liver. *Nat Commun* **11**: 2424. (2020).
61 Paradis, E. *et al.* ape 5.0: an environment for modern phylogenetics and evolutionary analyses in R. *Bioinformatics* **35**: 526-528. (2019).

Acknowledgments: Authors acknowledge support from the Shared Instrumentation Core Facility, Hangzhou Institute of Medicine (HIM), Chinese Academy of Sciences.

Funding:

National Key Research and Development Program of China 2022YFC3401402 (S, X)

National Key Research and Development Program of China 2023YFC3405100 (X, L)

National Natural Science Foundation of China T2188102 (W, T)

National Natural Science Foundation of China 22104133 (S, X)

National Natural Science Foundation of China 32201143 (X, L)

Hangzhou Institute of Medicine Chinese Academy of Sciences 2024ZZBS02 (S, X)

Zhejiang Provincial Natural Science Foundation of China LDQ23B050001 (S, X)

Zhejiang Provincial Natural Science Foundation of China LDQ24B020002 (X, L)

Zhejiang Provincial Natural Science Foundation of China LQ22B020007 (C, Z)

Author contributions:

Conceptualization: K.G., X.L., S.X. and W.T.

Methodology: T.L., L.H., Y.Z., W.Y., M.Z., Y.C., H.W., M.W., Y. Z., C.Z., W.W., Z.D., L. L. and P.Z.

Data analysis: B.L., S.L., Y.Z. and J.S.

Funding acquisition and Supervision: X.L., S.X. and W.T.

Writing – original draft & review & editing: K.G., X.L., S.X. and W.T.

Competing interests: The authors have filed a patent application (CN202410159815.8; Title: Methods for generating multifunctional CAR-Ms *in situ* and their application in immunotherapy; W.T., S.X., K.G., X.L., P.Z. and C.Z. are co-inventors) for some aspects of this work. The authors declare no competing interests.

Figure Legends

Fig. 1. **Design and functionality of CARs with variable ICDs for CAR-M.** (**a**) Schematic illustration of *in vitro* preparation of CAR-M containing pending CARs *via* mRNA PSβ-LNP. PSβ, phosphatidylserine and β-sitosterol. Flow cytometry analysis (**b**) and confocal images (**c**) of CARs expression on bone marrow-derived macrophages (BMDM) 24 h after mRNA PSβ-LNP transfection. Data are shown as mean ± SD (n = 4 technical replicates). CAR and nuclei were counterstained with HER2-AF647 (magenta) and Hoechst33258 (blue), respectively. Scale bar, 60 μm for the zoomed image. (**d**) Schematic procedures for functionality verification of CAR-M with pending CARs. (**e**) Normalized phagocytosis

of targeted luciferase-reported tumor cells by anti-HER2 CAR-Ms with pending ICDs in a series of E:T ratios at 2.5, 5 and 10. Data are shown as mean ± SD (n = 4 technical replicates per group for E/T = 2 or 5; n = 8 experimental wells comprising 4 technical replicates per condition from two independent experiments for E/T = 10). (**f**) Flow cytometry analysis of adhesion of controls or CAR-Ms and tumor cells 4 h after coincubation (E:T = 2:1). Macrophages: CD11b-FITC; Tumor cells: Sulfo-Cyanine5. (**g**) Confocal images of phagocytosis of HER2-beads by anti-HER2 CAR (CD3ζ) expressing THP-1 macrophage. HER2 beads and CAR-expressing THP-1 were stained with FITC (green) and DiD (magenta), respectively. Scale bar, 20 μm. Detected cytokines IL-12 (**h**) and IL-6 (**i**) in medium supernatant of controls or CAR-Ms and tumor cells 24 h after coincubation. Data are shown as mean ± SD (n = 3 technical replicates). Gene expression PCA (**j**) and heatmap (**k**) from bulk RNA-seq (n = 3 technical replicates) clustering from Blank, UTD, Empty, and CAR-Ms with ICDs (CD3ζ, CD40, CD46, CSF2R, Dectin1, and TLR4). Source data are provided as a Source Data file.

Fig. 2. Mutation of CAR ICD for enhancing persistence and CD47 recognition of CAR ECD for enhancing phagocytosis. (**a**) Schematic illustration of CAR optimization. (**b**) Flow cytometry analysis of CAR expression of ICD^{K} and $ICD^{K\text{-}R}$. (**c**) Normalized positive CAR-Ms with ICD^{K} or $ICD^{K\text{-}R}$ during continued target cell stimulation (n = 4 technical replicates for antigen stimulation; n = 3 technical replicates for no antigen stimulation). Normalized phagocytosis of luciferase-reported target tumor cells ((**d**) CT26-huERBB2^{+}-mCD47^{+} (n = 7 technical replicates in total from two independent

experiments); (**e**) SKOV3-huERBB2^{+}-huCD47^{+} (n = 4 technical replicates); and (**f**) HS578T-huERBB2^{-}-huCD47^{+}) by CAR-Ms (n = 4 technical replicates). E:T = 10:1. (**g**) Normalized phagocytosis of luciferase-reported non-target tumor cells (MDA-MB-231-huERBB2^{-}-CD47^{-}) by CAR-Ms (n = 4 technical replicates). E:T = 10:1. (**h**) Incucyte-based phagocytosis pictures of CT26-huERBB2^{+}-mCD47^{+}-eGFP^{+} by αCD47(CD3ζ) CAR-M or empty control within three days. E:T = 1:1. (**i**) Incucyte-based phagocytosis assay of HS578T-huERBB2^{-}-huCD47^{+}-eGFP^{+} by CAR-Ms or control within three days. Data are shown as mean ± SD for all panels. Source data are provided as a Source Data file.

Fig. 3. *In situ* programming of CAR-M *via* intraperitoneal administration of CAR-mRNA PSβ-LNP for tumor suppression. (**a**) Schematic experimental validation of PSβ-LNP targeting peritoneal macrophages. (**b**) Flow cytometry analysis of the proportion of eGFP-expressing ascites after infusion of eGFP-mRNA LNP. (**c**) eGFP and F4/80 double-positive proportion of the F4/80-positive population in **b** (from n = 3 mice). Data are presented as mean mean ± SD, and two-sided, unpaired Student's t test was used. (**d**) Immunofluorescence slice of tumor tissue from the CT26-luc syngeneic peritoneal dissemination mouse model after eGFP-mRNA PSβ-LNP infusion. Scale bar, 20 μm. White arrows indicate cells positive for both F4/80 and GFP. (**e**) Cell type composition of eGFP-positive cells analyzed by flow cytometry after infusion of eGFP-mRNA LNPs in both syngeneic mouse models. The minor other subset represents cells not captured by

the immune cell markers used in our panel. Data are presented as mean mean ± SD (from n = 3 mice), and statistical significance was determined by ordinary one-way ANOVA with Tukey's multiple comparisons test. (**f**) DIR signal distribution after intraperitoneal administration of DIR-labeled PSβ-LNP in CT26-luc syngeneic orthotopic colorectal cancer mouse model (from n = 3 mice). (**g**) Duration of CAR expression in $F4/80^+$ macrophages in the presence or absence of antigen stimulation in the CT26-luc syngeneic peritoneal dissemination mouse model (from n = 3 mice). Statistical significance was calculated using two-way ANOVA. (**h**) Schematic experimental design of CAR-mRNA PSβ-LNP programming of CAR-M *in situ* and *in vivo* bioluminescent images. (**i**) Quantified signal intensity of CT26-luc syngeneic murine model and Kaplan-Meier survival curves of mice after each treatment. Data were analyzed using the log-rank (Mantel-Cox) test (n = 5 mice). (**j**) *In vivo* bioluminescent images and (**k**) quantified signal intensity of CT26-luc syngeneic murine model and Kaplan-Meier survival curves of mice with macrophage depletion (n = 4 mice). Data were analyzed using the log-rank (Mantel-Cox) test. For all panels, ns = no significance. Source data are provided as a Source Data file.

Fig. 4. *In situ* programming of CAR-Ms activates the adaptive immune system. *In vivo* bioluminescent images (**a**) and tumor volume (**b**) of CT26-luc syngeneic rechallenged mice or naive mice (n = 4 mice) taken on the 65th day after prior CT26-luc inoculation. (**c**) Representative spot pictures and quantification data in IFNγ ELISPOT assay. Data are presented as mean ± SD (n = 3 technical replicates). (**d**) Tumor volume

of mice with adoptive splenocytes from CT26-luc syngeneic cured mice or naive mice (n = 5 mice). Adoptive transfer of splenocytes occurred one day before tumor cell inoculation. (**e**) Tumor volume of mice with adoptive splenocytes from CT26-luc syngeneic cured mice or naive mice (n = 5 mice). Adoptive transfer of splenocytes transferred 7 days after tumor cell inoculation. Statistical significance in Fig. 4b, 4d, and 4e was determined using the Mann–Whitney test. (**f**) Immunohistochemical analysis of CT26-luc tumor tissues resected in (**f**). Nuclei, blue; Macrophage (top, anti-F4/80, brown); T cell (down, anti-CD3, brown). Each panel shows low (left), medium (middle), and high (right) power views. (**g**) *In vivo* bioluminescent images and (**h**) bioluminescence imaging (BLI) fold change from post-treatment (day 18) to baseline (day 6) in the CT26-luc syngeneic peritoneal colorectal cancer mouse model (n = 3 for UTD/Empty, n =5 for CD3ζ, and n =4 for all other groups). (**i**) Kaplan-Meier survival curves of mice after each treatment (UTD, n = 3 mice; Empty, n = 4 mice; CD3ζ, n = 5 mice; CD40, n = 4 mice; TLR4, n = 4 mice; CD3ζ CD40, n = 4 mice; CD3ζ TLR4, n = 4 mice). Data were analyzed by using the log-rank (Mantel-Cox) test. (**j**) T cells phenotype analysis and M1/M2 ratios in ascites or tumors after CAR-mRNA LNP infusion (from n = 3 mice). Statistical significance was calculated using one-way ANOVA. For all panels, ns = no significance. Source data are provided as a Source Data file.

Fig. 5. CAR-Ms prime αPD-1 response in PD-1/PD-L1-resistant mouse models. *In vivo* bioluminescent images (**a**) and quantified signal intensity (**b**) of CT26-luc syngeneic mouse model with each treatment. (**c**) Kaplan-Meier survival curves of mice after each

treatment (UTD, n = 5 mice; αPD-1, n = 6 mice, CAR-M, n = 8 mice; Comb, n = 8 mice). Data were analyzed by using the log-rank (Mantel-Cox) test. (**d**) The ratio of intratumoral M1 and M2. (**e**) Percentage of intratumoral $CD4^+$ or $CD8^+$ T cells. For (**d**) and (**e**), data are presented as mean ± SD (from n = 3 mice), and statistical significance was determined using one-way ANOVA. (**f**) Multicolor immunofluorescence (nuclei, blue; CD3, white; CD11b, green; CD11c, red; F4/80, orange) of tumor tissue slices. Left panel is the tumor interior, and right panel is the tumor margin. Scale bar, 100 μm. (**g**) Levels of IL-12a in the blood across different groups (from n = 3 mice). Data are presented as mean ± SD, and statistical significance was calculated using one-way ANOVA. (**h**) Hierarchical clustering of TME cytokine concentration determined *via* Luminex multiplex cytokine assay under each treatment. *In vivo* bioluminescent images (**i**) and Kaplan-Meier survival curves (**j**) of the PAN02-luc syngeneic mouse model with each treatment (n = 6 mice). Data were analyzed by using the log-rank (Mantel-Cox) test. For all panels, ns = no significance. Source data are provided as a Source Data file.

Fig. 6. *In situ* programming of CAR-Ms leads to M1 polarization with enhanced PD-L1 and MHC I expression. (**a**) Schematic illustration of scRNA-seq analysis of the CT26-luc syngeneic mouse model. (**b**) Proportion of tumor-infiltrating immune cells labeled *via* scRNA-seq. (**c**) UMAP plot of scRNA-seq profiles from macrophages within the tumor. (**d**) Counts of clustered macrophages in groups. (**e**) UMAP plot of relative expression for the indicated gene (*Trem2*, *Nos2*, *Cd80*, *Cd274*). (**f**) Flow cytometry analysis of macrophage PD-L1 and H2-Kd expression in groups (**g)** Mean fluorescence intensity

(MFI) calculated from flow cytometry profiles of macrophage PD-L1 and H2-Kd**.** Data are presented as mean ± SD (n = 3 technical replicates). (**h**) Heatmap of MHC I and MHC II encoded gene expression in BMDMs after various CAR signal transduction. (**i**) Normalized MFI of macrophage PD-L1 and H2-Kd with NF-κBi (PDTC, 100 μM). Data are presented as mean ± SD (from n = 3 technical replicates). (**j**) Schematic representation of CAR signal transduction leading to upregulated PD-L1 and MHC I expression. (**k**) Recorded BLI of the CT26-luc syngeneic mouse model treated with UTD, PD-L1 siRNA, CAR-M, and combination therapy (n = 4 mice). (**l**) Counts of clustered T cells in groups. (**m**) Schema of the mechanism of potent synergy between tailored CAR-Ms and ICB. Source data are provided as a Source Data file.

Editorial Summary

Peritoneal metastasis remains a major clinical challenge due to the lack of effective therapeutic options . In this study, the authors present intraperitoneal programming of tailored chimeric antigen receptor macrophages (CAR-Ms) as a strategy against peritoneal metastasis.

Peer Review Information: *Nature Communications* thanks Marie Duhamel, Enzo Medico, Alice Dandrea and the other anonymous reviewer(s) for their contribution to the peer review of this work. [A peer review file is available.

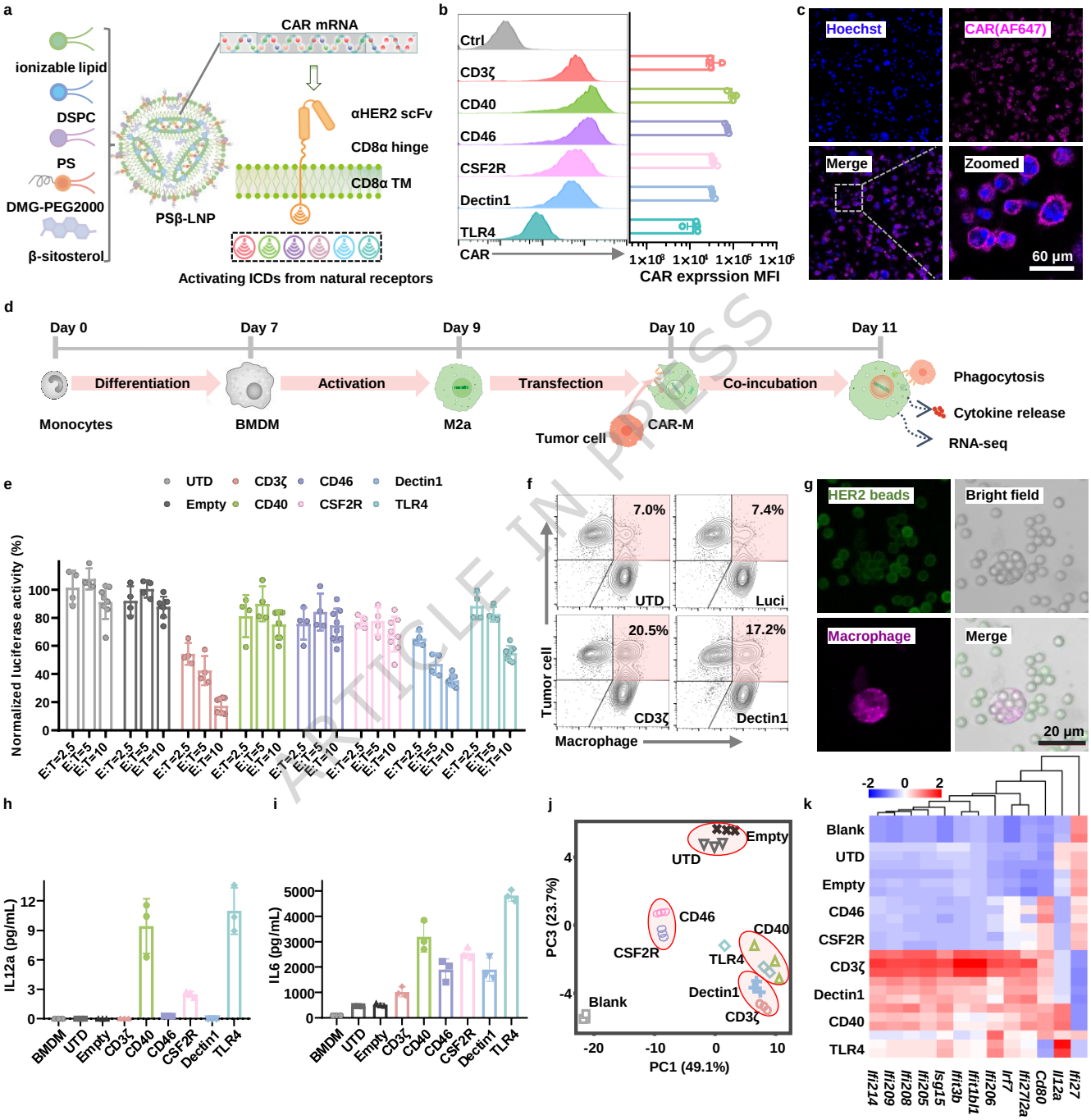

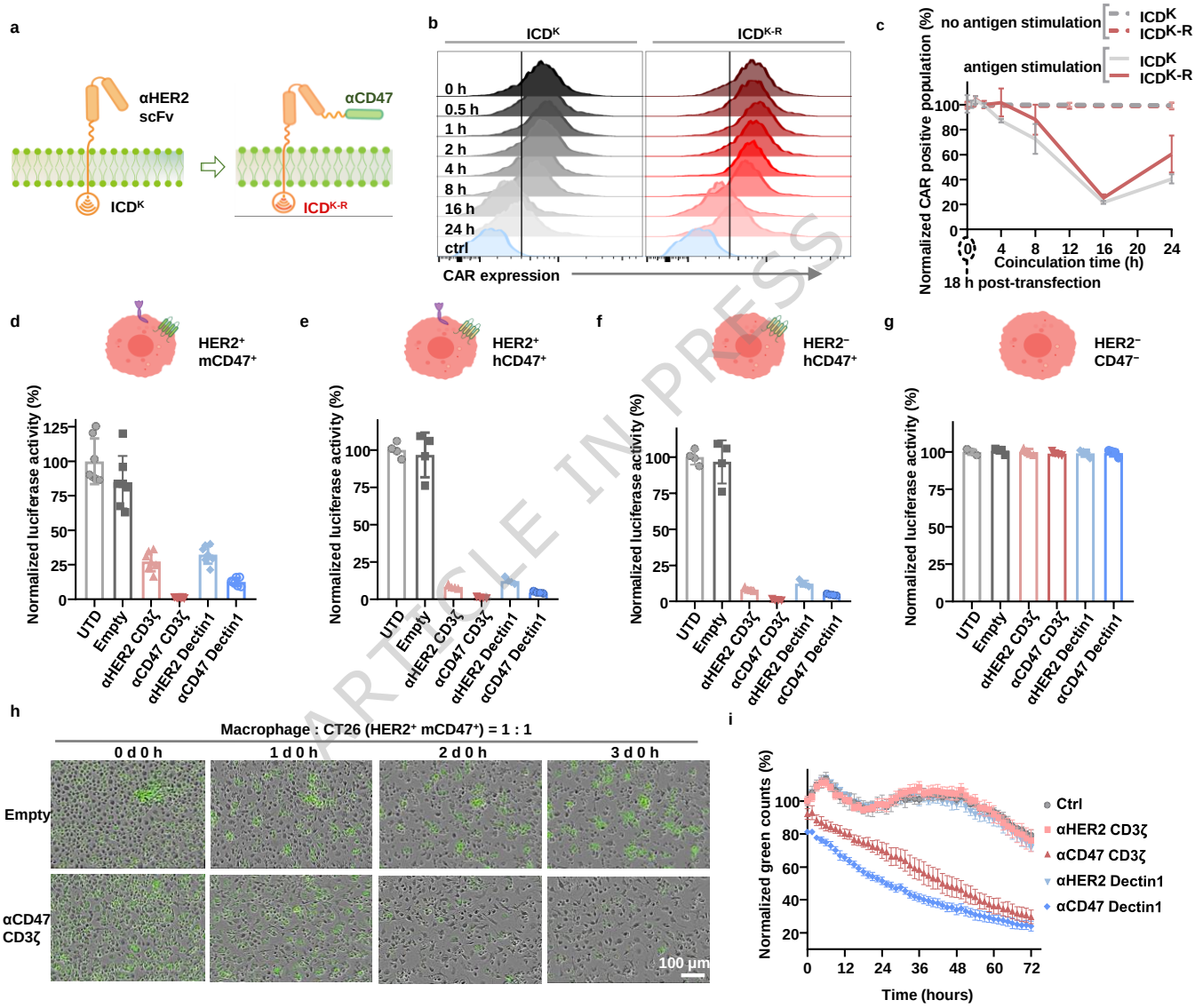
a
αHER2 scFv
αCD47
ICDK
ICDK-R
b
ICDK
ICDK-R
0 h
0.5 h
1 h
2 h
4 h
8 h
16 h
24 h
ctrl
CAR expression
c
no antigen stimulation
antigen stimulation
ICDK
ICDK-R
Normalized CAR positive population (%)
Coinculation time (h)
18 h post-transfection
d
HER2+ mCD47+
e
HER2+ hCD47+
f
HER2− hCD47+
g
HER2− CD47−
Normalized luciferase activity (%)
UTD
Empty
αHER2 CD3ζ
αCD47 CD3ζ
αHER2 Dectin1
αCD47 Dectin1
h
Macrophage : CT26 (HER2+ mCD47+) = 1 : 1
0 d 0 h
1 d 0 h
2 d 0 h
3 d 0 h
Empty
αCD47 CD3ζ
100 μm
i
Normalized green counts (%)
Time (hours)
Ctrl
αHER2 CD3ζ
αCD47 CD3ζ
αHER2 Dectin1
αCD47 Dectin1

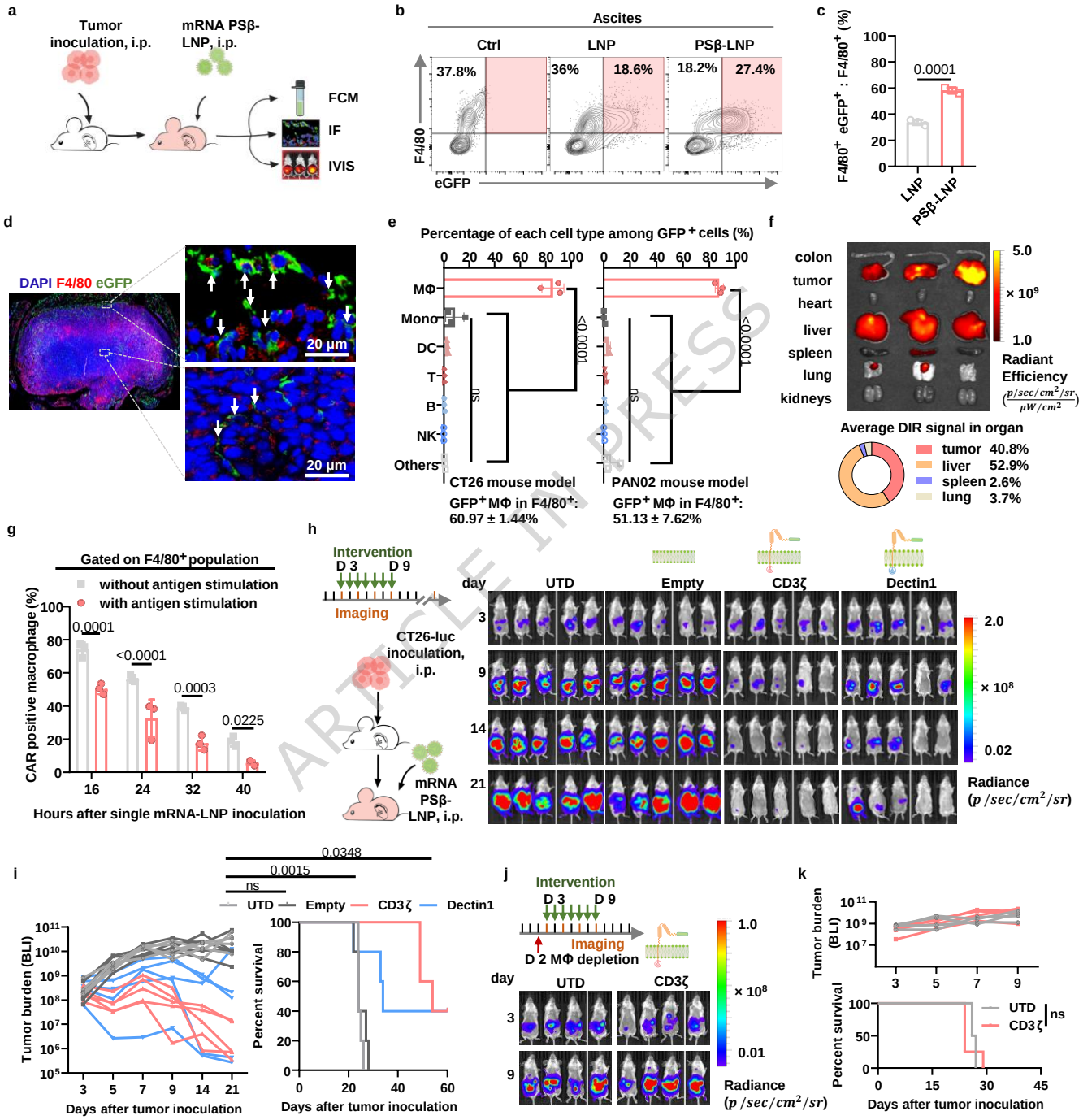
a
Tumor inoculation, i.p.
mRNA PSβ-LNP, i.p.
FCM
IF
IVIS
b
Ascites
Ctrl
LNP
PSβ-LNP
37.8%
36%
18.6%
18.2%
27.4%
F4/80
eGFP
c
F4/80+ eGFP+ : F4/80+ (%)
0.0001
LNP
PSβ-LNP
d
DAPI F4/80 eGFP
20 μm
20 μm
e
Percentage of each cell type among GFP+ cells (%)
MΦ
Mono
DC
T
B
NK
Others
<0.0001
ns
CT26 mouse model
GFP+ MΦ in F4/80+:
60.97 ± 1.44%
PAN02 mouse model
GFP+ MΦ in F4/80+:
51.13 ± 7.62%
f
colon
tumor
heart
liver
spleen
lung
kidneys
5.0
× 10^9
1.0
Radiant Efficiency
Average DIR signal in organ
tumor 40.8%
liver 52.9%
spleen 2.6%
lung 3.7%
g
Gated on F4/80+ population
without antigen stimulation
with antigen stimulation
CAR positive macrophage (%)
0.0001
<0.0001
0.0003
0.0225
Hours after single mRNA-LNP inoculation
h
Intervention
D 3
D 9
Imaging
CT26-luc inoculation, i.p.
mRNA PSβ-LNP, i.p.
day
UTD
Empty
CD3ζ
Dectin1
2.0
× 10^8
0.02
Radiance (p/sec/cm²/sr)
i
0.0348
0.0015
ns
UTD
Empty
CD3ζ
Dectin1
Tumor burden (BLI)
Days after tumor inoculation
Percent survival
Days after tumor inoculation
j
Intervention
D 3
D 9
Imaging
D 2 MΦ depletion
day
UTD
CD3ζ
1.0
× 10^8
0.01
Radiance (p/sec/cm²/sr)
k
Tumor burden (BLI)
Percent survival
UTD
CD3ζ
ns
Days after tumor inoculation

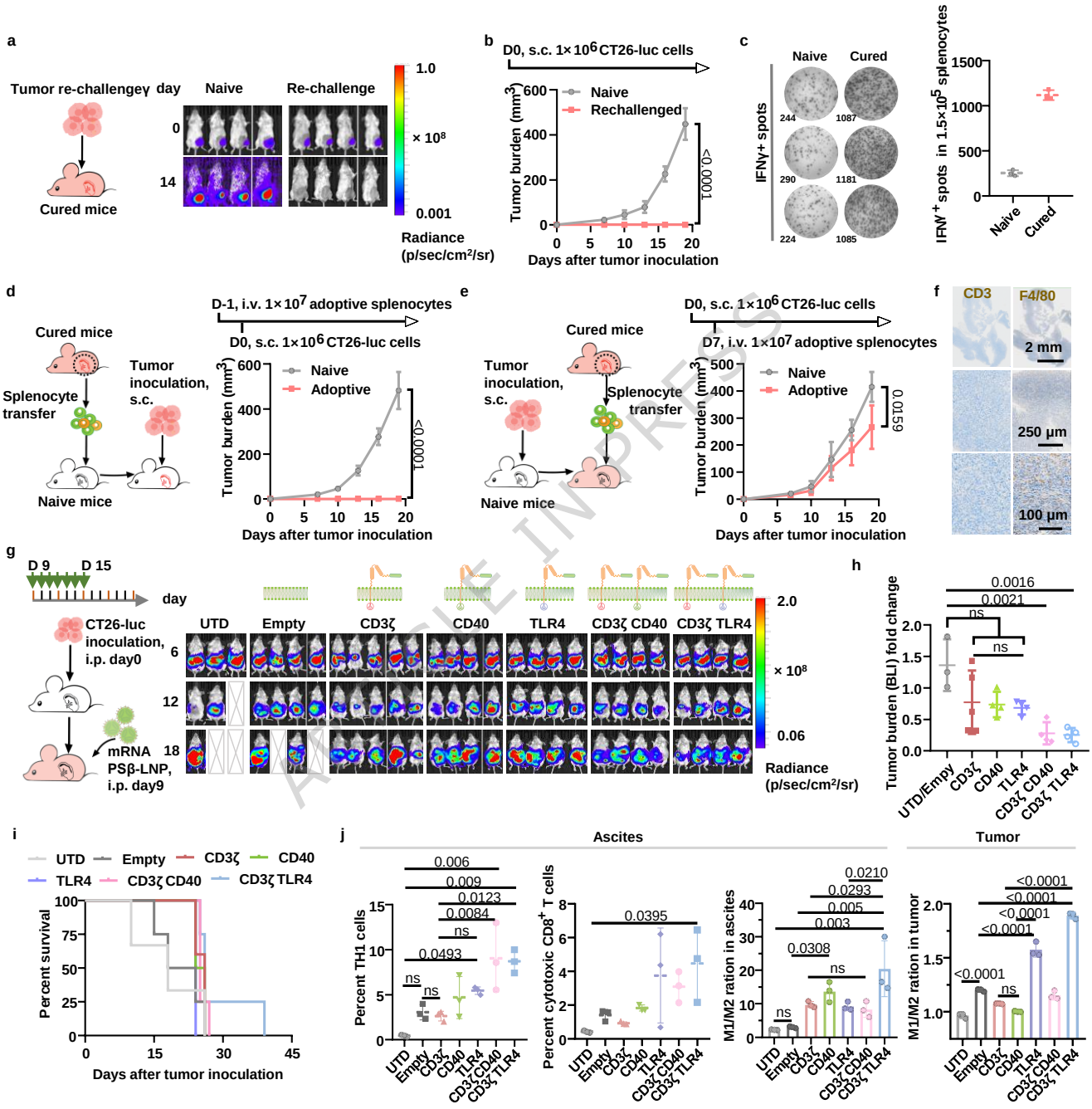

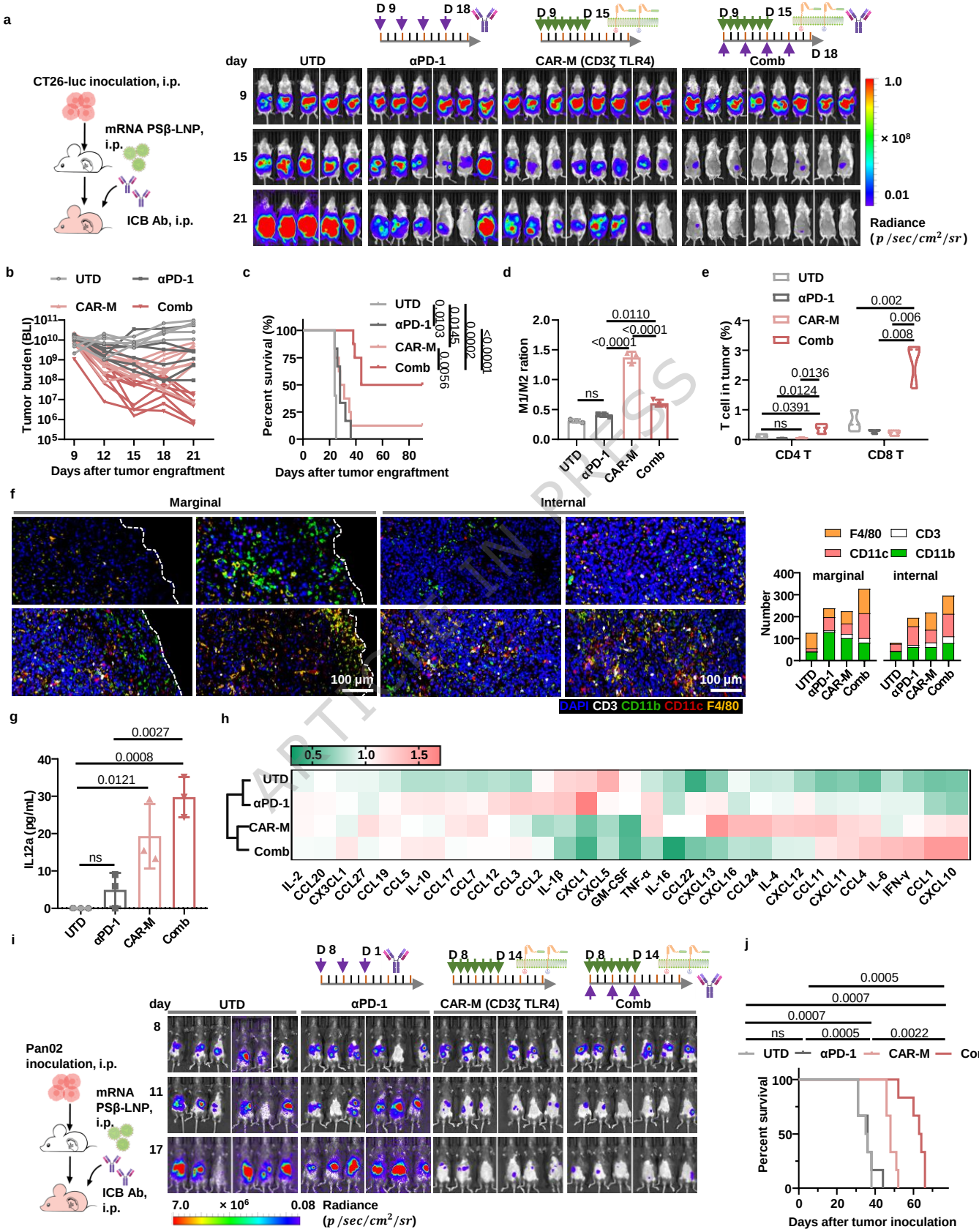
a
CT26-luc inoculation, i.p.
mRNA PSβ-LNP, i.p.
ICB Ab, i.p.
D 9
D 18
D 15
Comb
day
UTD
αPD-1
CAR-M (CD3ζ TLR4)
9
15
21
1.0
× 10^8
0.01
Radiance (p/sec/cm²/sr)
b
UTD
αPD-1
CAR-M
Comb
Tumor burden (BLI)
Days after tumor engraftment
c
Percent survival (%)
Days after tumor engraftment
0.0103
0.0145
0.0056
0.0002
≤0.0001
d
M1/M2 ration
ns
0.0110
<0.0001
<0.0001
e
T cell in tumor (%)
CD4 T
CD8 T
0.0136
0.0124
0.0391
ns
0.002
0.006
0.008
f
Marginal
Internal
100 μm
DAPI CD3 CD11b CD11c F4/80
F4/80
CD3
CD11c
CD11b
marginal
internal
Number
g
IL12a (pg/mL)
0.0027
0.0008
0.0121
ns
h
0.5
1.0
1.5
IL-2
CCL20
CX3CL1
CCL27
CCL19
CCL5
IL-10
CCL17
CCL7
CCL12
CCL3
CCL2
IL-1β
CXCL1
CXCL5
GM-CSF
TNF-α
IL-16
CCL22
CXCL13
CXCL16
CCL24
IL-4
CXCL12
CCL11
CXCL11
CCL4
IL-6
IFN-γ
CCL1
CXCL10
i
Pan02 inoculation, i.p.
mRNA PSβ-LNP, i.p.
ICB Ab, i.p.
D 8
D 1
D 14
day
8
11
17
7.0
× 10^6
0.08
Radiance (p/sec/cm²/sr)
j
0.0005
0.0007
0.0007
ns
0.0005
0.0022
Percent survival
Days after tumor inoculation

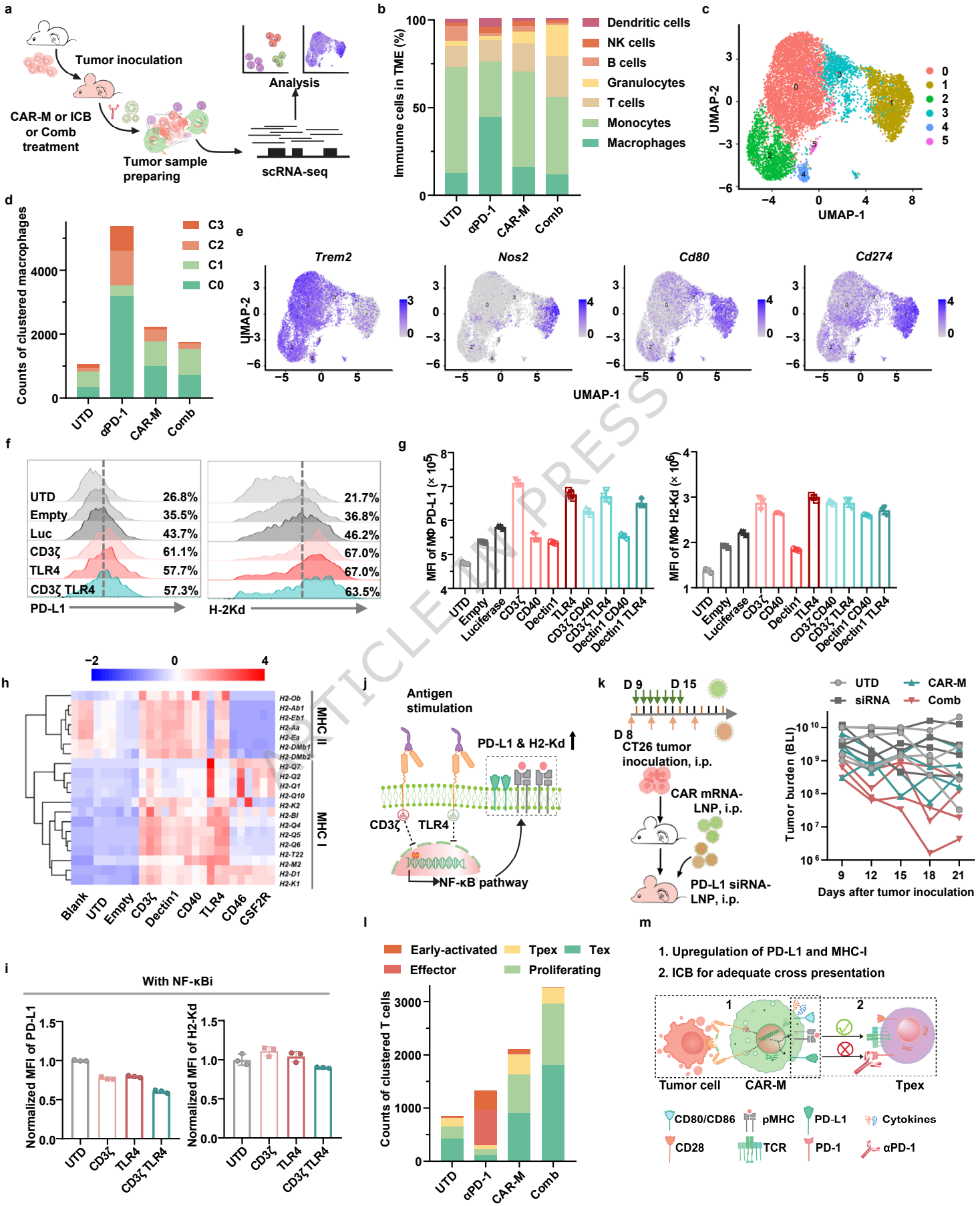
a
Tumor inoculation
CAR-M or ICB or Comb treatment
Tumor sample preparing
Analysis
scRNA-seq
b
Immunne cells in TME (%)
Dendritic cells
NK cells
B cells
Granulocytes
T cells
Monocytes
Macrophages
UTD
αPD-1
CAR-M
Comb
c
UMAP-2
UMAP-1
d
Counts of clustered macrophages
C3
C2
C1
C0
e
Trem2
Nos2
Cd80
Cd274
UMAP-2
UMAP-1
f
UTD 26.8% 21.7%
Empty 35.5% 36.8%
Luc 43.7% 46.2%
CD3ζ 61.1% 67.0%
TLR4 57.7% 67.0%
CD3ζ TLR4 57.3% 63.5%
PD-L1
H-2Kd
g
MFI of MΦ PD-L1 (× 10^5)
MFI of MΦ H2-Kd (× 10^6)
UTD
Empty
Luciferase
CD3ζ
CD40
Dectin1
TLR4
CD3ζ CD40
CD3ζ TLR4
Dectin1 CD40
Dectin1 TLR4
h
MHC II
MHC I
Blank
UTD
Empty
CD3ζ
Dectin1
CD40
TLR4
CD46
CSF2R
j
Antigen stimulation
PD-L1 & H2-Kd
CD3ζ
TLR4
NF-κB pathway
k
D 9
D 15
D 8
CT26 tumor inoculation, i.p.
CAR mRNA-LNP, i.p.
PD-L1 siRNA-LNP, i.p.
UTD
siRNA
CAR-M
Comb
Tumor burden (BLI)
Days after tumor inoculation
i
With NF-κBi
Normalized MFI of PD-L1
Normalized MFI of H2-Kd
UTD
CD3ζ
TLR4
CD3ζ TLR4
l
Early-activated
Tpex
Tex
Effector
Proliferating
Counts of clustered T cells
m
1. Upregulation of PD-L1 and MHC-I
2. ICB for adequate cross presentation
Tumor cell
CAR-M
Tpex
CD80/CD86
pMHC
PD-L1
Cytokines
CD28
TCR
PD-1
αPD-1